

1 **Controls on redox-sensitive trace metals in the Mauritanian oxygen minimum zone**

2 Insa Rapp^{1,2*}, Christian Schlosser¹, Jan-Lukas Menzel Barraqueta^{1,3}, Bernhard Wenzel¹, Jan Lüdke¹,
3 Jan Scholten⁴, Beat Gasser⁵, Patrick Reichert¹, Martha Gledhill¹, Marcus Dengler¹, and Eric P.
4 Achterberg¹

5 ¹Helmholtz Centre for Ocean Research Kiel (GEOMAR), Wischhofstr. 1-3, 24148 Kiel, Germany

6 ²Now at: Department of Biology, Dalhousie University, Halifax, Nova Scotia B3H 4R2, Canada

7 ³Department of Earth Sciences, Stellenbosch University, Stellenbosch, 7600, South Africa

8 ⁴Institute of Geosciences, Christian-Albrecht University Kiel (CAU), Otto-Hahn-Platz 1, 24118 Kiel,
9 Germany

10 ⁵International Atomic Energy Agency (IAEA), Environment Laboratories, 4 Quai Antoine 1er, 98012
11 Monaco

12 *Corresponding author. irapp@geomar.de

1 ABSTRACT

2 The availability of the micronutrient iron (Fe) in surface waters determines primary production, N₂
3 fixation and microbial community structure in large parts of the world's ocean, and thus plays an
4 important role in ocean carbon and nitrogen cycles. Eastern boundary upwelling systems and the
5 connected oxygen minimum zones (OMZs) are typically associated with elevated concentrations of
6 redox-sensitive trace metals (e.g. Fe, manganese (Mn) and cobalt (Co)), with shelf sediments typically
7 forming a key source. Over the last five decades, an expansion and intensification of OMZs has been
8 observed and this trend is likely to proceed. However, it is unclear how trace metal (TM) distributions
9 and transport are influenced by decreasing oxygen (O₂) concentrations. Here we present dissolved (d;
10 <0.2 μm) and leachable particulate (Lp; >0.2 μm) TM data collected at 7 stations along a 50 km
11 transect in the Mauritanian shelf region. We observed enhanced concentrations of Fe, Co and Mn
12 corresponding with low O₂ concentrations (<50 μmol kg⁻¹), which were decoupled from major
13 nutrients and nutrient-like and scavenged TMs (cadmium (Cd), lead (Pb), nickel (Ni) and copper
14 (Cu)). Additionally, data from repeated station occupations indicated a direct link between dissolved
15 and leachable particulate Fe, Co, Mn, and O₂. An observed dFe decrease from 10 to 5 nmol L⁻¹
16 coincided with an O₂ increase from 30 to 50 μmol kg⁻¹ and with a concomitant decrease in turbidity.
17 The changes in Fe (Co and Mn) were likely driven by variations in their release from sediment pore
18 water, facilitated by lower O₂ concentrations and longer residence time of the water mass on the shelf.
19 Variations in organic matter remineralization and lithogenic inputs (atmospheric deposition or
20 sediment resuspension; assessed using Al as indicator for lithogenic inputs) only played a minor role
21 in redox-sensitive TM variability. Vertical dFe fluxes from O₂-depleted subsurface to surface waters
22 (0.08–13.5 μmol m⁻² d⁻¹) driven by turbulent mixing and vertical advection were an order of
23 magnitude larger than atmospheric deposition fluxes (0.63–1.43 μmol m⁻² d⁻¹; estimated using dAl
24 inventories in the surface mixed layer) in the continental slope and shelf region. Benthic fluxes are
25 therefore the dominant dFe supply to surface waters on the continental margins of the Mauritanian
26 upwelling region. Overall, our results indicated that the projected future decrease in O₂ concentrations
27 in OMZs may result in increases in Fe, Mn and Co concentrations.

28 1. INTRODUCTION

29 The micronutrient iron (Fe) is essential for phytoplankton growth, but due to biological uptake
30 coupled with a low solubility and low supply rates, the availability of Fe is typically low in open ocean
31 surface waters (Bruland and Lohan, 2006). As a result, Fe limits primary production in high nitrate
32 low chlorophyll regions (Boyd, 2007) and regulates dinitrogen (N₂) fixation in (sub)-tropical waters
33 (Moore et al., 2009). Alongside Fe, other trace metals (TMs) such as cobalt (Co), manganese (Mn),
34 zinc (Zn) and copper (Cu) may (co-)limit phytoplankton growth and influence community
35 composition (Browning et al., 2017; Moore et al., 2013; Morel and Price, 2003; Saito et al., 2008).

1 Oxygen minimum zones (OMZs) are characterized by stable subsurface oxygen (O_2) minima, which
2 are maintained by a combination of enhanced O_2 consumption in the thermocline and a limited supply
3 of O_2 rich water masses (e.g. Brandt et al., 2015; Karstensen et al., 2008; Wyrski, 1962). Enhanced O_2
4 consumption is a result of elevated surface productivity caused by upwelling of nutrient-rich
5 subsurface waters in eastern boundary regions of the oceans through Ekman divergence, and intense
6 remineralization of sinking particles (e.g. Helly and Levin, 2004). Elevated organic matter supply and
7 water column O_2 depletion lead to enhanced benthic release of redox-sensitive elements by influencing
8 sediment diagenetic processes (Noffke et al., 2012; Severmann et al., 2010). Elevated concentrations
9 of sediment derived dissolved Fe, Co and Mn have been associated with lateral offshore advection in
10 O_2 depleted waters in the Arabian Sea, Pacific and Atlantic Ocean (Billler and Bruland, 2013; Hatta et
11 al., 2015; Hawco et al., 2016; Milne et al., 2017; Moffett et al., 2015; Noble et al., 2012).

12 Oxygen concentrations affect the distribution of redox-sensitive TMs by controlling oxidation rates
13 and influencing microbially mediated redox transformations. The reduced form of redox-sensitive
14 TMs, such as iron (Fe(II)), cobalt (Co(II)) and manganese (Mn(II)), have a higher solubility in
15 aqueous solutions than their oxidized forms (Fe(III), Co(III), Mn(III/IV)) (Liu and Millero, 2002;
16 Stumm and Morgan, 1995). Reduction of these metals occurs to a large extent in anoxic sediment pore
17 waters by microbial induced dissolution of particulate Fe(III) and Mn(III/IV) oxyhydroxides (Burdige,
18 1993; Chaillou et al., 2002; Froelich et al., 1979). Sediment pore waters are released to overlying
19 bottom waters by diffusion and bio-irrigation and during submarine groundwater discharge (Beck et
20 al., 2007; Elrod et al., 2004; Green et al., 2002). In contact with O_2 and other oxidants (e.g. nitrate
21 (Schlosser et al., 2018) and hydrogen peroxide (Moffett and Zika, 1987)), Fe(II) oxidizes to the poorly
22 soluble Fe(III) species, that are rapidly transformed into amorphous Fe oxyhydroxides or scavenged
23 onto particle surfaces (Moffett and Zika, 1987; Scholz et al., 2016; Wu and Luther, 1994). Mn(II) also
24 oxidizes to insoluble Mn(III/IV) oxides, but due to the slow abiotic oxidation kinetics, especially
25 under low O_2 conditions (e.g. von Langen et al., 1997), biotic oxidation by manganese oxidizing
26 bacteria is the main oxidation mechanism for Mn (Moffett, 1994; Sunda and Huntsman, 1988; Tebo
27 and Emerson, 1986). Co(II) removal is mainly associated with incorporation of Co into Mn oxides by
28 Co co-oxidation (Moffett and Ho, 1996).

29 Stabilizing mechanisms that prevent removal by scavenging and precipitation of Fe, Co and Mn are
30 organic ligand complexation (Elrod et al., 2004; Liu and Millero, 2002; Oldham et al., 2017; Parker et
31 al., 2007) and adsorption onto small slow sinking or neutrally buoyant particles (Lam et al., 2012).
32 Recent studies suggest a potentially important role for dynamic exchange processes between dissolved
33 and particulate phases of Fe, thereby influencing cycling and transport (Achterberg et al., 2018;
34 Fitzsimmons et al., 2017; Labatut et al., 2014; Milne et al., 2017). This was further indicated by Fe
35 isotope studies suggesting an equilibrium isotopic fractionation between the dissolved and particulate

1 phase in deep waters (Labatut et al., 2014) and the concomitant deepening of the dissolved and
2 particulate Fe plume that originated from a hydrothermal vent (Fitzsimmons et al., 2017).

3 Spatial and seasonal variations in TMs that are released from sediments, as well as ex-situ sediment
4 incubation experiments suggest a direct influence of bottom water and water column O₂ concentrations
5 on the distribution of Fe, Co and Mn (e.g. Biller and Bruland, 2013; Homoky et al., 2012). Differences
6 in benthic TM supply in field studies however suggest other factors such as sediment type, shelf
7 topography and organic matter supply also influence the benthic release of TMs (Homoky et al.,
8 2016). Ex-situ sediment incubation experiments offer a potential means to disentangle the influence of
9 O₂ concentrations relative to these controls (Homoky et al., 2012). These experiments, however, need
10 to be interpreted within the context of the confined conditions that eliminate potentially important
11 interactions in open systems, such as seawater exchange and mixing. Furthermore, they offer no
12 means to confidently evaluate controls on TM distributions in the pelagic water column.

13 In an attempt to resolve the controls on TM release and stabilization in OMZs we measured the
14 concentration of a suite of TMs along a 50 km long transect on the Mauritanian shelf in the Eastern
15 Tropical North Atlantic (ETNA). The Mauritanian shelf is associated with a major OMZ (minimum O₂
16 concentrations below 40 μmol kg⁻¹; Brandt et al., 2015) and is an important Fe source to the North
17 Atlantic Ocean (Milne et al., 2017). Furthermore, atmospheric dust deposition from the Saharan desert
18 can markedly elevate surface water Fe concentrations in the ETNA (Conway and John, 2014;
19 Rijkenberg et al., 2012). Recent observations suggest a decline in O₂ content of the oceans,
20 particularly in the northern and southern eastern Atlantic, and an expansion of OMZs, modulated by
21 the variability of our climate system (Hahn et al., 2017; Schmidtko et al., 2017; Stramma et al.,
22 2008b). These changes may result in changes in TM supply, and a mechanistic understanding of the
23 factors regulating TM release and stabilization in OMZs is therefore urgently needed. The aim of this
24 study was to evaluate the direct influence of variability in water column O₂ concentrations on the
25 distribution of redox-sensitive TMs and to identify responsible control mechanisms. Firstly, we assess
26 the fluxes of dFe in the OMZ to surface waters by vertical advection and diffusive mixing and
27 compared those to the atmospheric deposition flux of dFe. Secondly, we evaluate the importance of
28 redox and non-redox controls on Fe, Co and Mn by focusing on the influence of O₂ and particles on
29 the distribution of dissolved and leachable particulate TMs, including redox-sensitive (Fe, Co and Mn)
30 and nutrient-type and scavenged trace metals (aluminum (Al), lead (Pb), nickel (Ni), Cd and Cu).
31 Thirdly, we determine the influence of variability of the eastern boundary circulation and O₂
32 concentrations in regulating TM concentrations.

33 2. METHODS

34 2.1 Sampling

1 Samples were collected on RV Meteor cruise M107 in June 2014 during nine deployments at seven
2 locations (two stations were occupied twice) along a cross-shelf transect at 18°20'N on the
3 Mauritanian shelf in the ETNA (Figure 1). The bottom depths of stations varied between 50 m on the
4 shelf to 1136 m furthest off shore. Seawater sampling was carried out using a trace metal clean CTD
5 (TM-CTD, Sea-Bird SBE25) rosette frame equipped with 24 trace metal clean samplers (12 L, Ocean
6 Test Equipment (OTE)). The CTD frame was attached to plastic coated nonconductive steel cable and
7 deployed using a carousel auto-fire module (AFM, Sea-Bird) that closed the bottles at predefined
8 depths. After recovery, the bottles were transferred to a clean-laboratory container and pressurized to
9 0.2 bar overpressure using filtered N₂ gas. Samples were collected unfiltered for total dissolvable (TD)
10 TM measurements, and filtered using a 0.2 μm cartridge filter (Acropack 500, Pall) for dissolved (d)
11 TMs and iodide. Trace metal samples were collected in acid clean 125 mL low density polyethylene
12 (LDPE) bottles (Nalgene), and iodide samples in opaque 60 mL high density polyethylene (HDPE)
13 bottles (Nalgene). Trace metal samples were acidified to pH 1.9 using ultra clean HCl (UpA, Romil)
14 and stored double-bagged for >6 months before preconcentration and analysis. Samples for iodide
15 measurements were stored frozen at -20°C until analysis.

16 Samples for the determination of radium isotopes (²²³Ra; t_{1/2} = 11.4 d; ²²⁴Ra t_{1/2} = 3.7 d) were obtained
17 using in-situ filtration pumps (Challenger Oceanic) following the procedures described in Charette et
18 al. (2015) and Henderson et al. (2013). Briefly, each in-situ filtration pump was equipped with two
19 particle filters (70 μm; 1 μm) and two Mn dioxide (MnO₂) impregnated cartridges (CUNO Micro
20 Klean III acrylic) on which dissolved Ra adsorbs. In this work, ²²⁴Ra/²²³Ra ratios are shown, which
21 were analyzed from the first cartridge. The pumped water volumes varied between 1000 L and 1700 L
22 and flow rates were 10–15 L min⁻¹. For the determination of Ra in surface waters (~5 m water depth)
23 about 200–300 L of seawater was pumped into several 120 L plastic barrels followed by filtration over
24 MnO₂ coated acrylic fibers (Mn-fibers).

25 **2.2 Trace metal analysis**

26 Determination of Co, Mn, Fe, Cd, Pb, Ni and Cu was carried out as described in Rapp et al. (2017).
27 Briefly, samples were preconcentrated using an automated preconcentration device (SeaFAST,
28 Elemental Scientific Inc.) equipped with a cation chelating resin (WAKO; Kagaya et al., 2009).
29 Samples were UV-digested prior to preconcentration to breakdown metal-organic complexes, which
30 would cause an underestimation of the determined TM concentrations. Samples were buffered in-line
31 to pH 6.4 ± 0.2 using 1.5 M ammonium acetate buffer, before loading onto the resin. The pH buffer
32 was prepared using an ammonium hydroxide solution (22%, OPTIMA grade, Fisher) and acetic acid
33 (glacial, OPTIMA grade, Fisher) in de-ionized water (MilliQ, Millipore), adjusted to pH 8.5. Retained
34 TMs were eluted from the resin using 1 M distilled HNO₃ and collected in 4 mL polypropylene
35 scintillation vials (Wheaton). The acid was distilled from supra-pure HNO₃ (SpA grade, Romil) using
36 a sub-boiling PFA distillation system (DST-1000, Savillex). Preconcentration was performed within a

1 clean laboratory (ISO 5) and all sample and reagent handling was performed within the same
2 laboratory in an ISO 3 laminar flow bench with a HEPA filter unit. Preconcentrated samples were
3 analyzed by high resolution inductively coupled plasma-mass spectrometry (HR-ICP-MS, ELEMENT
4 XR, ThermoFisher Scientific) using isotope dilution for Fe, Cd, Pb, Cu and Ni and standard additions
5 for Co and Mn. SAFe reference seawater S and D2 were analyzed with each analytical run and
6 concentrations produced were in good agreement with consensus values (Table 1).

7 Leachable particulate (Lp) concentrations were calculated as the difference between total dissolvable
8 and dissolved concentrations. The limit of quantification (LOQ) for the Lp concentrations was
9 determined as the sum of the analytical standard deviations of TD and dissolved concentrations.
10 Extended uncertainty calculations were performed using the Nordtest approach (Naykki et al., 2015)
11 accounting for random as well as systematic errors (Rapp et al., 2017). The Lp fraction represents the
12 particulate fraction which is readily dissolvable in the acidified samples during storage at pH 1.9 for 6
13 months and therefore does not contain any refractory particle components. This more labile fraction of
14 particulate TMs mainly includes TMs in organic/biogenic particles, adsorbed to particle surfaces and
15 TM oxides/oxyhydroxides (Hurst et al., 2010).

16 **2.3 Aluminum measurements**

17 Aluminum concentrations were determined in surface water samples for all stations along the transect
18 and at two stations (3 and 8) for the entire water column. Samples were analyzed for Al using the
19 batch lumogallion method (Hydes and Liss, 1976). Acidified samples were buffered manually with a 2
20 M ammonium acetate buffer (Romil, UpA) to a pH between 5.1 and 5.2. The buffer was prepared
21 using ammonium hydroxide (Romil, UpA) and acetic acid (Romil, UpA) in de-ionized water (MilliQ,
22 Millipore). Buffered samples were spiked with a 2 mg L⁻¹ lumogallion (TCI) solution allowing the
23 complexing agent to be in excess. The lumogallion solution was prepared in 2 M ammonium acetate
24 buffer (Romil, UpA). After spiking, samples were heated up for 1.5 h at 80°C in an oven (Heratherm,
25 Thermo Scientific) and left to cool down overnight at room temperature to allow the formation of a
26 fluorescent Al complex. Samples were measured using a fluorescence spectrophotometer (Cary
27 Eclipse, Agilent). The samples were measured with an excitation and emission wavelength of 465 and
28 555 nm, respectively. The excitation and emission slits were set to 10. The plastic cuvettes used for the
29 measurements were pre-cleaned in a 2 M HCl (Trace metal grade, Fisher) for at least 24 h. In between
30 samples, the cuvette was thoroughly rinsed with de-ionized water followed by actual sample. The
31 same cuvette was used during an analytical session. All samples were analyzed in duplicate and the
32 concentrations calculated from the peak heights via standard addition. Samples and reagent natural
33 fluorescence was monitored by analyzing their content in the absence of the complexing agent. The
34 standards were prepared in low trace metal seawater from a 500 nmol L⁻¹ stock standard solution
35 prepared from a 1000 ppm Al standard solution (Merck Millipore). A typical calibration had the
36 following standard concentrations: 0, 10, 20, 40, and 60 nmol L⁻¹. GEOTRACES reference seawater

1 (GS) was run with a mean average Al value of $27.76 \pm 0.17 \text{ nmol L}^{-1}$ (n=4; consensus value
2 $28.2 \pm 0.2 \text{ nmol L}^{-1}$).

3 **2.4 Iodide measurements**

4 Frozen samples were defrosted overnight at room temperature prior to analysis for iodide by cathodic
5 stripping square wave voltammetry after Luther et al. (1988). The voltammetry unit consisted of a
6 voltammeter stand (663 VA, Metrohm), an autosampler (863 Compact Autosampler, Metrohm) and an
7 automatic burette (843 Pump Station, Metrohm) for automated spike addition. The system was
8 controlled by Computrace software (797 VA; Metrohm).

9

10 **2.5 Oxygen, salinity, nutrient, turbidity and chlorophyll fluorescence analysis**

11 Oxygen, salinity, nutrients, turbidity and chlorophyll fluorescence was measured during 62 CTD
12 deployments (including some repeated deployments at the same location) along the $18^{\circ}20'N$ transect
13 using a Sea-Bird SBE 9 CTD rosette system equipped with double sensor packages for O_2 , salinity and
14 temperature and 24 Niskin samplers (10 L; OTE). Turbidity and chlorophyll *a* were measured with a
15 combined Wetlabs turbidity and fluorescence sensor that was attached to the CTD. The output of both
16 sensors was corrected using the calibration provided by the manufacturer. Throughout this manuscript,
17 turbidity data are presented in nephelometric turbidity units (NTU). The noise level of the sensor in
18 our data set was found to be lower than 0.14 NTU. Oxygen sensor data were calibrated by Winkler
19 titration (Hansen, 2007; Winkler, 1888; Sommer et al., 2015) on 348 discrete water samples that were
20 collected from the OTE samplers. Oxygen sensor data was initially processed using calibration
21 coefficients provided by the manufacturer. Subsequently, O_2 sensor data were fitted to the O_2
22 concentrations determined by the Winkler titration method using linear functions for temperature, O_2
23 and pressure (i.e. depth). An uncertainty of $1.5 \mu\text{mol kg}^{-1}$ was determined for O_2 concentrations. On-
24 board nutrient measurements of nitrite (NO_2^-), nitrate (NO_3^-), phosphate (PO_4^{3-}) and silicic acid
25 (Si(OH)_4) of the discrete water samples were conducted using a QuAatro autoanalyzer (Seal
26 Analytical) according to Grasshoff et al. (1983).

27 Apparent Oxygen Utilization (AOU) was calculated as the difference between saturation
28 concentrations of O_2 and measured O_2 concentrations. The saturation concentration of O_2 was
29 calculated after the Weiss methods (Weiss, 1970) using the R package marelac (Soataert et al., 2016),
30 taking into account salinity and temperature.

31 **2.6 Radium analysis**

32 On-board the ship the Mn-cartridges and Mn-fibers were washed with Ra-free tap water to remove any
33 residual sea salt and particles. Ra was removed from the tap water by slowly ($<1 \text{ L min}^{-1}$) passing it
34 through a Mn-fiber filled cartridge. Afterwards, both cartridges and fibers were partially dried with

1 filtered compressed air to remove excess water. The samples were analyzed for ^{223}Ra , ^{224}Ra and ^{228}Th
 2 using a Radium Delayed Coincidence Counting System (RaDeCC) (Moore and Arnold, 1996). For the
 3 efficiency calibration of the RaDeCC, ^{227}Ac and ^{232}Th standard solutions were used, and the
 4 calibration followed the procedure described in Scholten et al. (2010) and Moore and Cai (2013).
 5 Counting errors were propagated following Garcia-Solsona et al. (2008). Excess ^{224}Ra ($^{224}\text{Ra}_{\text{ex}}$), i.e. the
 6 ^{224}Ra activity corrected for ^{228}Th -supported ^{224}Ra was calculated by subtracting the ^{228}Th activity from
 7 the ^{224}Ra activity. The ^{228}Th activity was measured three weeks after the first measurement of ^{224}Ra ,
 8 when the initial ^{224}Ra had decayed. As we measured only the first Mn cartridge and the Mn cartridges
 9 do not adsorb radium quantitatively, we report here only $^{224}\text{Ra}_{\text{ex}}/^{223}\text{Ra}$ ratios.

10 **2.7 Turbulence measurements and vertical flux calculations**

11 In order to advance understanding of the role of benthic Fe supply to the productive surface waters of
 12 the upwelling region, vertical diffusive fluxes (eq 1: left term, right hand side) and wind induced
 13 vertical advective fluxes (eq 1: right term, right hand side) were estimated. On the continental margin
 14 below the surface mixed layer, solutes are transferred vertically toward the near-surface layers by
 15 turbulent mixing processes and by vertical advection forced by Ekman divergence (e.g. Kock et al.,
 16 2012; Milne et al., 2017; Rhein et al., 2010; Steinfeldt et al., 2015, Tanhua and Liu, 2015):

$$17 \quad J_z = K_z \frac{\partial[TM]}{\partial z} + w \cdot \Delta[TM] \quad (1)$$

18 Here, K_z is the turbulent eddy diffusivity in $\text{m}^2 \text{s}^{-1}$, $\partial[TM]/\partial z$ the vertical gradient with depth (z) of the
 19 TM concentration $[TM]$ in $\mu\text{mol m}^{-4}$, $\Delta[TM]$ a TM concentration difference in $\mu\text{mol m}^{-3}$ and w
 20 represents vertical velocity in m s^{-1} . Average advective and diffusive TM fluxes were calculated for a
 21 depth interval from the shallow O_2 -depleted waters to surface waters. The exact depth interval varied
 22 for each station (see Table S2) due to differences in the depths where TM samples were collected. The
 23 upper depth (8–29 m) was always in layers with enhanced chlorophyll a fluorescence, although for
 24 some stations the upper depth was below the surface mixed layer.

25 Diffusive Fe fluxes were determined by combining TM concentration measurements from the TM-
 26 CTD stations with nearby measured microstructure profiles. The microstructure measurements were
 27 performed with an MSS90-D profiler (S/N 32, Sea & Sun Technology). The loosely-tethered profiler
 28 was optimized to sink at a rate of 0.55 m s^{-1} and equipped with three shear sensors, a fast-response
 29 temperature sensor, and an acceleration sensor, two tilt sensors and conductivity, temperature, depth
 30 sensors sampling with a lower response time. At TM-CTD stations with bottom depths less than 400
 31 m, 18 to 65 microstructure profiles were available at each station. At deeper stations, 5 to 12 profiles
 32 were used. Standard processing procedures were used to determine the rate of kinetic energy
 33 dissipation (ϵ) of turbulence in the water column (see Schafstall et al. (2010) for detailed description).
 34 Subsequently, K_z values were determined from $K_\rho = \Gamma \epsilon N^{-2}$ (Osborn, 1980), where N is stratification

1 and Γ is the mixing efficiency for which a value of 0.2 was used. The use of this value has recently
 2 been shown to yield good agreement between turbulent eddy diffusivities determined from
 3 microstructure measurements and from tracer release experiments performed in our study region
 4 (Köllner et al., 2016). The 95% confidence intervals for station-averaged K_ρ values were determined
 5 from Gaussian error propagation following Schafstall et al. (2010). Finally, diffusive fluxes were
 6 estimated by multiplying station-averaged K_ρ with the vertical gradient of the respective TM solute,
 7 implicitly assuming $K_z=K_\rho$.

8 The vertical advective flux by Ekman divergence requires determination of vertical velocity in the
 9 water column that varies with depth and distance from the coast line. Convincing agreement between
 10 vertical velocities derived from Ekman divergence following Gill (1982) determined from
 11 scatterometer winds and from helium isotope disequilibrium within the Mauritanian and Peruvian
 12 coastal upwelling regions was found by Steinfeldt et al. (2015) (see their Fig. 4). In their study,
 13 vertical velocities were parameterized as (Gill, 1982):

$$14 \quad w = \frac{\tau_y}{\rho f L_r} e^{-x/L_r} \quad (2)$$

15 where τ_y represents the alongshore wind stress, ρ the density of sea water, x the distance from
 16 maximum Ekman divergence taken here as the position at 50 m bottom depth on the shelf and L_r the
 17 first baroclinic Rossby radius. The parameterization results from considering the baroclinic response
 18 of winds parallel to a coastline in a two-layer ocean (Gill, 1982). The baroclinic Rossby radius
 19 $L_r = f^{-1} \sqrt{g \frac{\rho_2 - \rho_1}{\rho} \frac{H_1 H_2}{H_1 + H_2}}$ ($\rho_{1/2}$ and $H_{1/2}$ are density and thickness of the surface and lower layer,
 20 respectively) was found to be 15 km from hydrographical data collected during the cruise. Similar
 21 values were determined by Steinfeld et al. (2015) in the same region. Using average alongshore wind
 22 stress from satellite data (0.057 Nm^{-2} , determined from daily winds from Remote Sensing Systems
 23 ASCAT C-2015, version v02.1 (Ricciardulli and Wentz, 2016) at $18^\circ 22.5' \text{N}$, $016^\circ 7.5' \text{W}$ using
 24 $\tau_y = \rho_{air} C_d v^2$, where v represents alongshore wind, C_d is drag coefficient for which 1.15×10^{-3} was
 25 used (e.g. Fairall et al., 2003) and ρ_{air} is density of air) for June 2014, maximum vertical velocities of
 26 $3.7 \times 10^{-5} \text{ m s}^{-1}$ were determined for the shelf region (50 m water depth), which decayed offshore to
 27 $1.7 \times 10^{-6} \text{ m s}^{-1}$ at the position of the 1000 m isobath at 18°N . As these vertical velocities describe the
 28 magnitude of upwelling at the base of the mixed-layer, additional corrections need to be considered for
 29 deeper depths. Here, we approximated the vertical decay of w as a linear function which diminishes at
 30 the ocean floor.

31 The calculation of the vertical advective flux supplying solutes from the shallow O_2 -depleted waters to
 32 surface waters requires knowledge of a concentration difference $\Delta[\text{TM}]$ associated with the upwelling
 33 flux. Ideally, the vertical length scale over which the concentration difference is determined can be

1 diagnosed as the TM concentration variance divided by its mean vertical gradient (e.g. Hayes et al.,
2 1991). However, in our study TM concentration time series data are not available. Previous studies
3 have used a vertical length scale of 20 m to calculate the concentration differences between the target
4 depth and the water below (e.g. Hayes et al., 1991; Steinfeldt et al., 2015; Tanhua and Liu, 2015). For
5 our calculations, we chose to use a smaller length scale of 10 m following Hayes et al. (1991) which
6 results in vertical advective TM flux presumably on the lower side of possible values.

7 **2.8 Figures**

8 All figures were produced in R (version 3.4.3). Data gridding in figures 2 and 3 was performed using
9 the Tps function within the fields package in R (Nychka et al., 2016).

10 **3. RESULTS & DISCUSSION**

11 **3.1 Oceanographic settings of the study area**

12 The cruise was conducted in June 2014 along a transect crossing a narrow shelf off the Mauritanian
13 coast at 18°20'N. The vertical structure of the OMZ in this region is characterized by a deep OMZ at
14 about 400 m depth, and a shallow OMZ at about 100 m depth (Brandt et al., 2015). Coastal upwelling
15 of nutrient-rich deep water occurs as a result of offshore transport of surface waters caused by a
16 Northeast Trade wind component parallel to the coast. While north of 20°N upwelling persists
17 throughout the year, upwelling south of 20°N, including the Mauritanian upwelling region, undergoes
18 seasonal changes in upwelling strength (Barton et al., 1998), with strongest upwelling occurring
19 between December and April. The seasonal variability is mainly driven by changes in wind forcing
20 associated with the migration of the Intertropical Convergence Zone (Lathuilère et al. 2008). During
21 the cruise period, cold upwelled waters with temperature less than 20°C were still present on shelf and
22 upper continental slope (Thomsen et al., 2019, their Fig. 1) indicating active upwelling.

23 The eastern boundary circulation consists of the Mauritania Current (MC, Fig. 1) flowing poleward at
24 the surface against the equatorward winds and of the Poleward Undercurrent (PUC) flowing in the
25 same direction at depths between 50 and 300 m (Barton, 1989; Klenz et al., 2018; Mittelstaedt, 1983;
26 Peña-Izquierdo et al., 2015). Both currents supply cold, O₂ and nutrient-rich waters of predominantly
27 South Atlantic origin (South Atlantic Central Water, SACW) to the coastal upwelling region (e.g.
28 Mittelstaedt, 1991; Mittelstaedt, 1983; Peña-Izquierdo et al., 2015). In response to the changing winds,
29 the eastern boundary circulation likewise exhibits a pronounced seasonal variability (Klenz et al.,
30 2018; Stramma et al., 2008a). The strongest poleward flow is observed during the relaxation period
31 between May and July when alongshore, upwelling-favorable winds weaken but wind stress curl is at
32 its maximum (Klenz et al., 2018). During the upwelling season in boreal winter, the circulation more
33 closely resembles the classical eastern boundary circulation regime, with a weak poleward
34 undercurrent flowing beneath an equatorward coastal jet (Klenz et al., 2018; Kounta et al., 2018). At

1 deeper levels (300–500 m depth), flow was found to be equatorward during both seasons. The shallow
2 (<300 m depth) boundary circulations turn offshore at the southern flank of the Cape Verde frontal
3 zone (CVFZ) (e.g. Tomczak, 1981; Zenk et al., 1991) at about 20°N, separating SACW from more
4 saline and O₂-rich Central Waters formed in the North Atlantic (NACW). The circulation in June 2014
5 was typical for a relaxation period characterized by strong poleward flow over the shelf and the upper
6 continental slope between the surface and 250 m depth (Klenz et al., 2018; Thomsen et al., 2019).
7 During the later parts of the cruise, the core of the MC moved offshore and reduced poleward flow
8 was observed near the shelf break. Periods of elevated northward flow on the Mauritanian shelf
9 inhibits the onshore near-bottom supply of low oxygen but nitrate-rich waters onto the shelf with
10 consequences for benthic nitrogen cycling (Yücel et al., 2015).

11 Meridional sections of water mass properties and O₂ concentrations from around 18°N showed that
12 waters with an enhanced SACW proportion advected from the south as well as NACW coming from
13 the north, have higher O₂ concentrations than the ambient waters (Klenz et al., 2018). The mixture of
14 SACW and NACW waters found in the thermocline particularly during boreal winter, previously
15 identified as a regional water mass and termed the Cape Verde SACW (SACW_{cv}) by Peña-Izquierdo
16 et al. (2015), is a signature of an older water mass with lower O₂ concentrations than those of SACW
17 or NACW due to a longer residence time and O₂ consumption through remineralization. Elevated
18 pelagic oxygen consumption levels at the Mauritanian continental margin were recently determined by
19 Thomsen et al. (2019). During the transition period in May through July upper Central Waters (50–
20 300 m depth) are dominated by SACW accounting for 80–90 % of the water masses in the boundary
21 current region (Klenz et al., 2018).

22 The SACW transported poleward within the boundary circulation is supplied by the zonal North
23 Equatorial Counter Current (NECC) and North Equatorial Under Current (NEUC), which flow
24 eastward at about 5°N (Brandt et al., 2015) before diverging into a northward and a southward flowing
25 branch in front of the African coast.

26 As a result of interactions between tidal currents, topography and critically sloping upper continental
27 slope topography (e.g. Eriksen, 1982), the Mauritanian upwelling region is known for elevated
28 nonlinear internal wave activity resulting in enhanced mixing in the water column of the upper slope
29 and shelf region (Schafstall et al., 2010). Vertical fluxes of nutrients driven by mixing processes are
30 amongst the largest reported in literature, however lower than in the Celtic Sea (Tweddle et al., 2013)
31 and the lower St. Lawrence Estuary (Cyr et al., 2015).

32 The CTD and microstructure deployments were performed along the east-west transect in the period
33 June 8 to June 27 (2014) (Fig. 1). Oxygen concentrations reached a deep minimum of 40–50 μmol kg⁻¹
34 at about 400 m and a shallow minimum of 30–50 μmol kg⁻¹ at about 50–100 m (Fig. 2), which is in
35 agreement with previous studies (Brandt et al., 2015; Thomsen et al., 2019). Mixed layer depths

1 ranged between 10 and 22 m during the cruise. Salinity was highest at the surface (ca. 36.02) and
2 generally decreased with depth to a minimum of 34.71 at around 1000 m. Nitrate (NO_3^-)
3 concentrations in the surface mixed layer varied between 0.1 and $11.3 \mu\text{mol L}^{-1}$ and phosphate (PO_4^{2-})
4 between 0.15 and $0.91 \mu\text{mol L}^{-1}$. NO_3^- and PO_4^{2-} concentrations increased with depth to a maximum of
5 47.6 and $3.2 \mu\text{mol L}^{-1}$, respectively (Fig. 2).

6 Over a time period of 19 days, two trace metal stations along the transect at water depths of 170 m
7 (18.23°N , 16.52°W , 1st deployment: June 12, 2nd deployment: June 21) and 189–238 m (18.22°N ,
8 16.55°N , 1st deployment: June 24, 2nd deployment: June 26) were reoccupied. Minimum O_2
9 concentrations of $30 \mu\text{mol kg}^{-1}$ observed before June 15 increased to $50 \mu\text{mol kg}^{-1}$ after June 19 or
10 June 24, depending on the location. This oxygenation event, captured in ocean glider measurements is
11 discussed in detail by Thomsen et al. (2019). Variability in oxygen concentrations observed further
12 offshore was attributed to physical transport of SACW into the region (Thomsen et al. 2019). In
13 contrast, closer to the coast, enhanced pelagic oxygen consumption rates were determined that
14 significantly contribute to the variability in observed oxygen concentrations (Thomsen et al., 2019).
15 Short-term variability in oxygen concentrations has also been observed further south in nearshore
16 Senegalese waters where an anoxic event was likely attributed to the offshore advection of a decaying
17 diatom bloom (Machu et al. 2019).

18 The sediments in the study area contain a large amount of carbonate, biogenic silica and quartz
19 (Hartman et al. 1976). The fraction of sand and mud varies largely depending on bottom depth, with
20 sand comprising between 7 and 70% of the dry weight (Dale et al., 2014). The particulate organic
21 carbon (POC) content varies between 0.55 wt% at shallow depth (66 and 90 m) and increases to
22 3.3 wt% at 1108 m depth (Schroller-Lomnitz et al., 2019). A more detailed description of the
23 sediments underlying our study region and sediment parameters collected on the same cruise,
24 including Fe(II) concentrations and Fe/Al ratios, are given in Schroller-Lomnitz et al. (2019).

25 **3.2 Spatial distributions of dissolved and leachable particulate trace metals**

26 Dissolved Fe and LpFe concentrations ranged between $0.97\text{--}18.5 \text{ nmol L}^{-1}$ and $1.6\text{--}351 \text{ nmol L}^{-1}$,
27 respectively (Fig. 3a, b). Surface waters (5–29 m) had lowest dFe ($0.97\text{--}4.7 \text{ nmol L}^{-1}$) and LpFe (1.6--
28 35.9 nmol L^{-1}) concentrations, whereas highest concentrations were present on the shelf close to the
29 seafloor (up to 18.5 nmol L^{-1} dFe and 351 nmol L^{-1} LpFe). Enhanced concentrations of both Fe
30 fractions at any given station were observed at depths with low O_2 concentrations (30--
31 $60 \mu\text{mol O}_2 \text{ kg}^{-1}$). A similar distribution pattern was observed for dCo, with concentrations between
32 0.069 and $0.185 \text{ nmol L}^{-1}$ (Fig. 3c). In contrast, LpCo concentrations varied from below the limit of
33 quantification (LOQ) up to $0.179 \text{ nmol L}^{-1}$ and were generally highest in surface waters and close to
34 the coast (Fig. 3d). Compared to dFe, the concentration range of dCo was much narrower and
35 enhanced concentrations were observed over a broader depth range and further offshore.

1 Surface dFe and dCo concentrations were low, presumably due to enhanced biological uptake. No
2 clear increasing trend in dFe and dCo with depth was observed, indicating that processes other than, or
3 in addition to, remineralization influenced their distributions. Elevated concentrations were found
4 close to the sediments and within low O₂ waters. This suggested a benthic source of Fe and Co under
5 O₂-depleted conditions, and offshore transport along O₂-depleted water filaments, which is in
6 agreement with previous studies (e.g. Baars and Croot, 2015; Hatta et al., 2015; Noble et al., 2012).
7 Our sharper onshore-offshore gradient of dFe concentrations compared to dCo in O₂-depleted waters
8 shows that oxidation and removal mechanisms/scavenging rates were faster for Fe than Co (Noble et
9 al., 2012). Previously reported dFe concentrations in coastal regions of the tropical North Atlantic
10 were lower than we observed, between 0.5–6.3 nmol L⁻¹ (Hatta et al., 2015; Milne et al., 2017; Wuttig
11 et al., 2013). However, all these samples were collected at a greater distance from the coast. In the
12 near-coastal Oregon and Washington shelf bottom water dFe concentrations were similar to our study
13 under equivalent O₂ concentrations (18.7–42.4 nmol L⁻¹ dFe, 42–61 μmol kg⁻¹ O₂; Lohan and Bruland,
14 2008), whereas in the euxinic waters from the Peruvian shelf region, dFe concentrations were more
15 than an order of magnitude higher, exceeding 200 to 300 nmol L⁻¹ (Schlosser et al., 2018; Scholz et al.,
16 2016). Similar dCo concentrations to our study were observed in the North and South Atlantic, with
17 highest concentrations of ~0.16 nmol L⁻¹ present within O₂-depleted waters (Noble et al., 2012; Noble
18 et al., 2017).

19 Dissolved Mn concentrations ranged between 0.46–13.8 nmol L⁻¹ and LpMn between below LOQ–
20 4.4 nmol L⁻¹ (Fig. 3e, f). Highest dMn and LpMn concentrations were observed in surface waters,
21 generally decreasing with depth. Additionally, concentrations were highest on the shelf and decreased
22 offshore. The dMn concentrations were generally elevated within and below the deeper O₂-depleted
23 waters with 0.70–1.34 nmol L⁻¹ compared to 0.46–0.91 nmol L⁻¹ just above. The increased dMn
24 concentrations within the deeper O₂-depleted waters (~350–500 m depth) indicate a benthic source,
25 similar to Fe and Co, which is in accordance with previous studies (Noble et al., 2012). However, in
26 the shallow O₂-depleted waters (~50–200 m depth), this effect is not resolvable due to high surface
27 concentrations, which were maintained by photo-reduction of Mn oxides to soluble Mn(II) that
28 prevents loss of Mn from solution (Sunda and Huntsman, 1994). Reported dMn concentrations in the
29 North and South Atlantic were lower than in our study, with concentrations <3.5 nmol L⁻¹ in surface
30 waters and around 0.5–1 nmol L⁻¹ dMn within the OMZ (Hatta et al., 2015; Noble et al., 2012; Wuttig
31 et al. 2013). As for dFe, these lower reported values can also be explained by sampling stations
32 positioned at further distance from the coast and removal of dMn via biological oxidation processes
33 with distance from the source (Moffett and Ho, 1996).

34 Dissolved Cd and Ni concentrations were lowest in surface waters with 0.022–0.032 nmol Cd L⁻¹ and
35 2.6–2.8 nmol Ni L⁻¹, and showed an increasing trend with depth to maximum values of 0.60 nmol L⁻¹
36 and 5.8 nmol L⁻¹, respectively (Fig. 3g, m). Leachable particulate Cd concentrations were between

1 below LOQ and 0.20 nmol L^{-1} , and LpNi concentrations between below LOQ and 1.7 nmol L^{-1} . A
2 large fraction of Ni (72–100%) was present in the dissolved form. The majority of LpNi samples were
3 below the LOQ (>70% of the data) and LpNi is therefore not included in Fig. 3. LpCd concentrations
4 were highest close to the coast and decreased offshore (Fig. 3h). In surface waters close to the coast
5 the LpCd fraction was dominant with up to 84.3% of the entire Cd pool (d + Lp). The fraction of LpCd
6 in surface water beyond the shelf break (including stations 2, 1 and 9) contributed still up to 54.3% of
7 the Cd pool, whereas below 50 m only 0–12.8% of TDCd was in the Lp phase beyond the shelf break.
8 In contrast to Fe, Co and Mn, no increases in Cd and Ni were observed near the seafloor and within
9 the O_2 -depleted waters indicating that Cd and Ni concentrations are mainly controlled by
10 remineralization of sinking organic matter, which is typical for these two nutrient-like TMs (Biller and
11 Bruland, 2013). Similar distributions with concentrations between 0 and 1000 m water depth ranging
12 from $\sim 2\text{--}5.5$ and $\sim 0\text{--}0.55 \text{ nmol L}^{-1}$ for dNi and dCd, respectively, were observed during the
13 GEOTRACES transect GA03_w in the tropical North Atlantic (Mawji et al., 2015; Schlitzer et al.,
14 2018).

15 Dissolved Cu concentrations in surface waters ranged between $0.63\text{--}0.81 \text{ nmol L}^{-1}$ (Fig. 3i).
16 Concentrations increased with depth to around 1.37 nmol L^{-1} at 700 m depth close to the seafloor,
17 whereas highest observed concentrations further offshore were 0.95 nmol L^{-1} at the greatest sampled
18 depth of 850 m. These results indicate that in addition to remineralization processes of sinking
19 biogenic particles, the distribution of Cu is influenced by inputs from the seafloor. This is in
20 accordance with previous studies, suggesting that Cu is released from continental shelf sediments
21 under oxic and moderately reducing conditions (Biller and Bruland, 2013; Heggie, 1982), whereas no
22 increase in Cu concentrations near the seafloor was observed at low bottom water O_2 concentrations
23 ($\text{O}_2 < 10 \mu\text{mol L}^{-1}$; Johnson et al., 1988). A decrease in Cu concentrations in the bottom boundary layer
24 was also reported with a seasonal decrease in O_2 in summer from a minimum of $70 \mu\text{mol L}^{-1} \text{ O}_2$ in
25 May to $40 \mu\text{mol L}^{-1} \text{ O}_2$ in August, suggesting a decrease in sedimentary release of Cu (Biller and
26 Bruland, 2013). In strongly reducing sediments and the presence of H_2S , Cu forms inorganic sulfides
27 and precipitates, which may explain reduced sedimentary Cu release under low bottom water O_2
28 concentrations (Biller and Bruland, 2013). Therefore, the sediment source of dCu might show a
29 different dependency on bottom water O_2 concentrations than dFe, dCo and dMn explaining the
30 distinct distribution of dCu. Concentrations of LpCu were between below the LOQ to 0.61 nmol L^{-1}
31 with enhanced levels at station 4 close to the coast and at mid depths of the three stations furthest
32 offshore (9, 5 and 2) (Fig. 3j).

33 Observed dPb concentrations were lowest in the surface waters at $9\text{--}14 \text{ pmol L}^{-1}$ and increased with
34 depth to $29\text{--}86 \text{ pmol L}^{-1}$ below 600 m depth (Fig. 3k). Lead is not considered a nutrient-like TM (e.g.
35 Boyle et al., 2014), but our observations indicate a release of Pb from sinking particles following
36 remineralization. The concentration range and depth distribution is similar to reported distributions

1 further offshore at about 21°W (Noble et al., 2015). These authors suggested that increased
 2 concentrations of up to 70 pmol L⁻¹ between 600 and 800 m depth were related to the influence of
 3 Mediterranean Outflow Waters (MOW). Additionally, increased Pb concentrations in proximity to
 4 sediments have been attributed to the benthic release of historic Pb through reversible scavenging from
 5 particles and the release of dPb associated with Fe/Mn oxyhydroxides during reductive dissolution of
 6 those oxides in anoxic sediments (Rusiecka et al., 2018). The major source of Pb to the ocean is
 7 atmospheric dust deposition from anthropogenic emissions (Bridgestock et al., 2016; Nriagu and
 8 Pacyna, 1988; Veron et al., 1994) with a recent indication of reduced anthropogenic Pb inputs to
 9 surface waters in the eastern tropical Atlantic under the North African dust plume (Bridgestock et al.,
 10 2016). Low surface water concentrations on the Mauritanian shelf indicate low atmospheric inputs of
 11 Pb to this region. LpPb was below the LOQ—27 pmol L⁻¹, and the distribution of LpPb was similar to
 12 that of LpFe, with subsurface maxima within O₂-depleted waters (Fig. 3l) and may indicate increased
 13 scavenging of dPb in these layers which might be associated with Fe containing particles.

14 In general, sediment derived TM concentrations decrease with distance from the shelf and with time
 15 that passed since the water mass has been in contact with the sediments due to water mass mixing and
 16 removal processes such as precipitation and scavenging (Bruland and Lohan, 2006). Radium isotopes
 17 can be used as a tracer for benthic sources. The major source of Ra to the ocean is input from
 18 sediments through the efflux of pore water, sediment resuspension, and submarine groundwater
 19 discharge (Moore, 1987; Moore and Arnold, 1996; Rama and Moore, 1996). Due to the distinctive
 20 half-lives of the different Ra isotopes (e.g. ²²⁴Ra (t_{1/2} = 3.66 d) and ²²³Ra (t_{1/2} = 11.4 d)) and their
 21 conservative behaviour in seawater, it is possible to quantify the time that has passed since a parcel of
 22 water was in contact with the sediments using the following equation by Moore (2000):

$$\left(\frac{A_{224}}{A_{223}}\right)_{obs} = \left(\frac{A_{224}}{A_{223}}\right)_i \frac{e^{-\lambda_{224}\tau}}{e^{-\lambda_{223}\tau}} \quad (3)$$

23 solved for water mass age (τ):

$$\tau = \frac{\ln\left(\frac{A_{224}}{A_{223}}\right)_{obs} - \ln\left(\frac{A_{224}}{A_{223}}\right)_i}{\lambda_{223} - \lambda_{224}} \quad (4)$$

24 where A_{224}/A_{223} is the activity ratio of ²²³Ra and ²²⁴Ra, with the subscript *obs* for the observed seawater
 25 ratio and the subscript *i* for the initial groundwater endmember ratio, and λ_{223} and λ_{224} are the decay
 26 constants in d⁻¹ for ²²³Ra and ²²⁴Ra. The ratio ²²⁴Ra/²²³Ra is not affected by dilution assuming there is
 27 no mixing with waters having significantly different ²²⁴Ra/²²³Ra ratios.

28 Highest ²²⁴Ra_{ex}/²²³Ra activity ratios were observed close to the seafloor (Fig. 3n). The average
 29 ²²⁴Ra_{ex}/²²³Ra ratio in proximity to the sediment source (< 20 m above seafloor) was 4.1 ± 0.7 and was
 30 similar to reported ratios for shelf waters off South Carolina (²²⁴Ra_{ex}/²²³Ra = 4.1 ± 0.7; Moore, 2000).

1 The $^{224}\text{Ra}_{\text{ex}}/^{223}\text{Ra}$ ratios decreased away from their benthic source due to decay ($^{224}\text{Ra}_{\text{ex}}/^{223}\text{Ra} = 0\text{--}0.5$
2 in surface waters). Ratios close to the seafloor were relatively constant along the transect at bottom
3 depths <600 m, whereas dFe, dCo and dMn concentrations varied largely in the bottom samples. This
4 suggests that factors, which are not influencing the Ra distribution, impacted the distributions of dFe,
5 dCo and dMn, with a likely influence of enhanced O_2 concentrations reducing sediment release or
6 increasing removal rates of these metals at water depths between 200 and 400 m. At around 800 m
7 bottom depth, $^{224}\text{Ra}_{\text{ex}}/^{223}\text{Ra}$ ratios were slightly elevated and coincided with increased dCo, dFe, dMn
8 and dCu concentrations despite O_2 concentrations $>70 \mu\text{mol kg}^{-1}$. This suggests that the enhanced TM
9 concentrations at this location were influenced by a strong sediment source which may be related to
10 the presence of a benthic nepheloid layer as indicated by an increase in turbidity in proximity to the
11 seafloor. An elevated $^{224}\text{Ra}_{\text{ex}}/^{223}\text{Ra}$ ratio of 3.5 ± 0.6 was observed at about 16.65°N and 80 m water
12 depth (bottom depth 782 m) and coincided with a local maximum of dFe, dMn and dCo and reduced
13 O_2 concentrations. These observations indicate that the waters with the local maximum of dFe, dMn
14 and dCo have been in relatively recent contact (12–20 days assuming initial pore water $^{224}\text{Ra}_{\text{ex}}/^{223}\text{Ra}$
15 ratios between 18–38; Moore, 2007) with sediments, likely originated from south of our transect as a
16 result of a strong poleward flow (Klenz et al., 2018), and that the dynamic current system in this
17 region can cause local and short-term variability in the transport of sediment derived TMs.

18 **3.3 Classification of different groups of trace metals based on principal component analysis**

19 Principal Component Analysis (PCA) was performed (using the RDA function within the vegan
20 package in R; Oksanen et al., 2017) to investigate different groups and correlations in the data set.
21 Dissolved TMs (Fe, Mn, Co, Ni, Pb, Cu and Cd), nutrients (silicic acid, nitrate and phosphate),
22 dissolved O_2 , Apparent Oxygen Utilization (AOU), depth and iodide concentrations (Supplementary
23 Fig. S1) were utilized in the PCA. Radium data were not included in the PCA, as the number of
24 available data points for $^{224}\text{Ra}_{\text{ex}}/^{223}\text{Ra}$ was much lower than for the other parameters. Surface waters
25 shallower than 50 m were excluded from the PCA to remove the influence of localized atmospheric
26 deposition and photochemical processes, which in particular influence Mn and iodide distributions.
27 The PCA generated three principal components (PC) with eigenvalues larger than 1, with PC1
28 explaining 53.6% and PC2 25.5% of the total variance in the dataset (together 79.1%). Inclusion of
29 PC3 in the analysis explained only 6.8% more of the variance.

30 The first PC group is formed by dCd, dCu, dNi and dPb (Fig. 4), which are associated with depth,
31 AOU, nitrate and phosphate. This indicates that the distribution of Cd, Cu, Ni, and potentially Pb, are
32 controlled by organic matter remineralization processes. This is in agreement with strong Pearson
33 correlations $R > 0.9$ for the relationships of dCd and dNi with depth, nitrate and silicic acid
34 (Supplementary Material, Table S1). Weaker correlations with major nutrients were observed for dPb
35 ($R > 0.6$) and dCu ($R > 0.4$), potentially due to additional remineralization or removal mechanisms for
36 these elements (e.g. prior atmospheric inputs and water mass transport, Pb; sediments, Cu and Pb, and

1 scavenging). The second group of TMs is composed of dFe, dCo and dMn that are associated with
2 elevated iodide and turbidity, and low dissolved O₂ (Fig. 4). Iodide (I⁻) is the reduced form of iodine
3 (I₂), which is typically present as iodate (IO₃⁻) in oxygenated subsurface water. Both I forms are present
4 as soluble anions in seawater. Due to a relatively high redox potential (pE ~10), iodine is one of the
5 first redox-sensitive elements to undergo reduction under suboxic conditions and is therefore a useful
6 indicator for active reductive processes (Rue et al., 1997). Despite their role as micronutrients, Fe, Mn
7 and Co do not correlate with nutrients indicating that processes other than remineralization controlled
8 their distributions.

9 The anti-correlation with O₂ (also shown in Fig. S2) and correlation with iodide support the notion that
10 Fe, Co and Mn distributions were strongly influenced by water column O₂ concentrations, presumably
11 through: (i) enhanced benthic metal fluxes from anoxic sediments, and (ii) decreased oxidation rates in
12 the overlying water column under O₂-depleted conditions. This is also supported by elevated benthic
13 Fe(II) fluxes observed at the seafloor within the shallow OMZ, with benthic fluxes of 15–27 μmol m⁻²
14 d⁻¹ (Schroller-Lomnitz et al., 2018).

15 Variability in the redox-sensitive metals, Fe, Mn and Co, were not fully explained by either O₂ or
16 iodide concentrations; Pearson correlations with O₂ were -0.55, -0.61 and -0.58, respectively
17 (Supplementary Material, Table S1). As shown before, other factors such as, for example, water mass
18 mixing and age, the amount and type of particles present, and remineralization all likely impact their
19 dissolved concentrations. Consequently, such a complex chain of factors and processes means that one
20 variable alone is unlikely to explain the behaviour of Fe, Mn, and Co.

21 **3.4 Influence of the different sources of Fe, Mn and Co**

22 The main sources of TMs in our study region are sedimentary release and atmospheric dust deposition
23 (e.g. Rijkenberg et al., 2012). Also release of TMs via organic matter remineralization may have an
24 important influence on the distribution of TMs. In the following, we discuss the relative influence of
25 remineralization, atmospheric dust deposition and sedimentary release on the supply of Fe, Co and Mn
26 to surface waters.

27 *3.4.1 Remineralization*

28 To quantify the influence of remineralization for dFe, we employed dFe to carbon (dFe/C) ratios
29 (carbon was calculated using AOU, with an AOU/carbon ratio of 1.6; Martin et al., 1989). Surface
30 data, where O₂ was over-saturated (due to biological O₂ production), were excluded. Dissolved Fe/C
31 ratios for the entire transect varied between 15 and 74 μmol mol⁻¹. These results agree with those for
32 shelf-influenced waters with dFe/C ratios of 13.3–40.6 μmol mol⁻¹ further south at 12°N (Milne et al.,
33 2017). Reported ratios for the North Atlantic, further away from the shelf were lower and ranged
34 between 4 and 12.4 μmol mol⁻¹ (Fitzsimmons et al., 2013; Milne et al., 2017; Rijkenberg et al., 2014).

1 To estimate the amount of dFe being derived by remineralization, we assume a dFe/C ratio of 4–
2 12 $\mu\text{mol mol}^{-1}$ from organic matter remineralization, similar to the observed dFe/C ratios in the open
3 ocean close to our study area without a strong shelf influence. These offshore ratios may still be
4 influenced by an atmospheric source of dFe, which would result in an overestimation of dFe/C ratios
5 from remineralization and thereby an overestimation of the fraction of remineralized dFe. Apart from
6 additional inputs, the dFe/C ratios are influenced by the respective Fe/C stoichiometry in the sinking
7 organic matter and removal of dFe by scavenging. Furthermore, it is not clear if the offshore ratios can
8 be transferred to a location close to the coast, as the balance between remineralization and scavenging
9 processes might be different due to differences in phytoplankton productivity and particle load. Hence,
10 this approach only provides a broad estimate of the relative influence of remineralization on the
11 distribution of dFe in the study area.

12 We obtain a range between $5 \pm 3\%$ and $54 \pm 27\%$ for dFe being derived from remineralization
13 processes with lowest values observed on the shelf at 34 m depth at station 4 ($5 \pm 3\%$) and highest
14 values estimated beyond the shelf break at Stn 9 at 213 m depth ($54 \pm 27\%$) and Stn 2 at 450 m depth
15 ($52 \pm 26\%$). However, no clear increase in the contribution of remineralized dFe to total dFe with
16 depth or distance to the coast was observed. For example at depths between 35 and 200 m, our
17 estimates of dFe from remineralization ranged between $10 \pm 5\%$ and $51 \pm 25\%$ with high values of up
18 to $41 \pm 20\%$ at 50 m depth at station 7 close to the coast, whereas relatively low values of $19 \pm 9\%$
19 were observed at 89 m at station 2. These results indicate that, locally, remineralization can be an
20 important control on dFe concentrations, but that the contribution varies largely with additional
21 important controls, often dominating over remineralization.

22 Similar analysis for dCo/C ratios revealed an increased importance of an additional source close to the
23 shelf. Observed dCo/C ratios ranged between 0.81 and $2.2 \mu\text{mol mol}^{-1}$. The larger ratios were
24 observed close to the coast and decreased further offshore. Overall, the observed ratios were somewhat
25 higher than reported cellular ratios of phytoplankton in the North Atlantic of $0.5\text{--}1.4 \mu\text{mol mol}^{-1}$
26 (Twining et al., 2015). However, relatively constant dCo/C ratios beyond the shelf break (dCo/C:
27 $0.82\text{--}1.09 \mu\text{mol mol}^{-1}$, stations 2, 5 and 9) that are similar to cellular ratios of phytoplankton suggest a
28 large influence of remineralization on dCo beyond the shelf break, whereas enhanced ratios close to
29 the coast suggest an additional benthic source. Due to the lack of comparable data of offshore dCo/C
30 ratios and the multiple processes influencing this ratio (varying phytoplankton nutrient stoichiometry
31 and scavenging), we did not use these values to estimate the remineralized dCo fraction.

32 The distribution of Mn was not predominantly determined by biological uptake and remineralization
33 processes in our study region. In contrast, dMn/C ratios were largely influenced by photoreduction in
34 the surface (Sunda and Huntsman, 1994), removal via biotic oxidation and formation of Mn oxides at
35 depth (Tebo et al., 2004). Therefore, we did not assess remineralization processes for Mn using dMn/C
36 ratios.

3.4.2 Atmospheric deposition

Aluminum is present as a relatively constant fraction of ~8.15 wt% in the continental crust (Rudnick and Gao, 2006), is supplied to open ocean surface waters mainly by atmospheric deposition (Orians and Bruland, 1986) and is not considered to be taken up by phytoplankton (apart from a small amount being incorporated into siliceous diatom frustules; Gehlen et al., 2002). Therefore, dAl in the surface mixed layer is used as a tracer for atmospheric deposition to the surface ocean (Measures and Brown, 1996; Measures and Vink, 2000). The atmospheric input in the study region is mainly influenced by North African/Saharan mineral dust with only a small contribution of anthropogenic sources which differ greatly in TM composition and solubilities from mineral dust (Baker et al., 2013; Patey et al., 2015; Shelley et al., 2015). Close to continental shelves, Al can also be supplied by sediment resuspension in addition to atmospheric input (Menzel Barraqueta et al., 2018; Middag et al., 2012; Moran and Moore, 1991). Enhanced aerosol optical depth above our study region (Supplementary Fig. S3&4) indicates high dust loading at the time of our cruise. Our dAl concentrations in surface water ranged between 30 and 49 nmol L⁻¹ and LpAl between 3.4 and 18.2 nmol L⁻¹. Dissolved Al concentrations decreased with depth (Fig. 8), indicating that Al was released by aeolian dust deposition to surface waters and removed through scavenging at depth (Orians and Bruland, 1985).

Dissolved atmospheric deposition fluxes can vary largely depending on the aerosol solubility, which is dependent on aerosol source, atmospheric aerosol processing during transport and dissolution in surface waters (Jickells, 1999). Here, atmospheric dFe fluxes were calculated using the dAl inventory in the surface mixed layer, a residence time of dAl of 0.65 ± 0.45 years as reported for the Canary Current System (Dammshäuser et al., 2011), and a ratio of 0.31 for dust derived dissolved Fe/Al (Buck et al., 2010). This approach is independent of the fractional solubility of Al, as we do not account for total atmospheric deposition fluxes, and only use the already dissolved fraction of Al. However, this approach is dependent on the ratio of Fe/Al from dissolution of aerosols. This ratio, however, is not clearly defined and can vary between different dust sources and deposition pathways, such as wet or dry deposition (e.g. Shelley et al., 2018). In our study region, dry deposition is the dominant deposition pathway, as it is located north of the Intertropical Convergence Zone and precipitation is minimal < 0.001 g/cm⁻³ (NASA). Here, we utilized a ratio observed for total aerosol samples in the remote North Atlantic from a Saharan dust source (Buck et al. 2010). Soluble ratios under the Saharan dust plume were however lower for all leach media (Fe/Al: 0.051–0.25; Shelley et al. 2018), indicating that the ratio of 0.31 utilized here, might result in an overestimation of the dFe flux estimates. This approach also assumes that dAl is only supplied to the surface ocean via atmospheric deposition. Vertical fluxes of Al from sediment resuspension are unlikely to contribute significantly to concentrations of dAl in surface waters here as dAl concentrations decreased with depth, indicating removal of dAl via scavenging.

1 Mean atmospheric dFe fluxes of the individual stations were 0.63–1.4 $\mu\text{mol m}^{-2} \text{d}^{-1}$ (Fig. 5,
2 Supplementary Table S2), values similar to reported fluxes close to our study region of
3 2.12 $\mu\text{mol m}^{-2} \text{d}^{-1}$ further north between 22.5–25°N and 26.5–27.5°W (Rijkenberg et al., 2012) and
4 0.120 $\mu\text{mol m}^{-2} \text{d}^{-1}$ around 20°N close to the African coast (Ussher et al., 2013). The uncertainty in the
5 residence time of dAl, however, creates a large uncertainty in calculated fluxes resulting in a lowest
6 flux of 0.37 $\mu\text{mol m}^{-2} \text{d}^{-1}$ when using the largest estimated residence time of 1.1 years and a highest
7 flux of 4.65 $\mu\text{mol m}^{-2} \text{d}^{-1}$ when using the shortest estimated residence time of 0.2 years. In fact, a
8 residence time of 3 months has been shown to give similar results for total Al atmospheric deposition
9 fluxes as modeling studies (Menzel Barraquetta et al., 2019). Low residence times of a few months
10 have also been suggested for Al and Fe in areas with a large dust deposition including our study region
11 (e.g. Croot et al. 2004, Dammshäuser et al., 2011). Therefore, we suggest that the atmospheric dFe
12 flux is more likely to be closer to the upper range of our flux estimates. However, the atmospheric
13 deposition fluxes using a short residence time may be larger than the annual average since the dust
14 load is highest between June and August in our study area (Supplementary Fig. S4).

15 3.4.3 Vertical trace element fluxes to surface waters

16 The vertical diffusive and advective fluxes of dFe from shallow O₂ depleted waters to surface waters
17 with enhanced chlorophyll *a* fluorescence were determined to assess the potential Fe contribution to
18 phytoplankton growth from suboxic waters (Fig. 5). A detailed summary of the individual dFe flux
19 estimates, and their uncertainties is given in Supplementary Table S2.

20 Vertical dFe fluxes increased by two orders of magnitude from 70 km offshore to the shallow shelf
21 region. On the shelf (bottom depth: 50 m), an elevated mean dFe flux of 13.5 $\mu\text{mol m}^{-2} \text{d}^{-1}$ was
22 estimated. The contribution from vertical advection (upwelling) here (11.99 $\mu\text{mol m}^{-2} \text{d}^{-1}$) was an
23 order of magnitude larger than the diffusive flux (1.56 $\mu\text{mol m}^{-2} \text{d}^{-1}$). Our estimate agrees with a
24 reported vertical dFe flux of 16 $\mu\text{mol m}^{-2} \text{d}^{-1}$ on the shelf at 12°N (Milne et al., 2017). Average
25 estimates from the upper continental slope and the lower shelf region (stations 3, 7 and 8, bottom
26 depth: 90–300 m) were between 1 $\mu\text{mol m}^{-2} \text{d}^{-1}$ and 2.5 $\mu\text{mol m}^{-2} \text{d}^{-1}$. Here, the vertical diffusive fluxes
27 dominated (0.72–1.75 $\mu\text{mol m}^{-2} \text{d}^{-1}$) and were about a factor of three larger than vertical advective
28 fluxes (0.22–0.68 $\mu\text{mol m}^{-2} \text{d}^{-1}$). The elevated diffusive fluxes at the upper continental slope and lower
29 shelf region are due to enhanced diapycnal mixing that originates from tide – topography interactions
30 (Schafstall et al., 2010). At 170 m depth of the repeated station (3), vertical dFe flux estimates were
31 2.3 $\mu\text{mol m}^{-2} \text{d}^{-1}$ and 1.4 $\mu\text{mol m}^{-2} \text{d}^{-1}$, respectively. The differences in the two values are due to
32 differences in the strength of turbulent mixing during the two station occupations. For the offshore
33 stations 2 and 9 (bottom depth > 500 m), mean dFe fluxes were 0.08–0.16 $\mu\text{mol m}^{-2} \text{d}^{-1}$ with similar
34 contributions of diffusive and advective fluxes. However, one offshore station (station 5) exhibited
35 elevated dFe fluxes of 1.3 $\mu\text{mol m}^{-2} \text{d}^{-1}$ with a large contribution of the diffusive flux term
36 (1.03 $\mu\text{mol m}^{-2} \text{d}^{-1}$). Here, diapycnal mixing was determined from only 5 microstructure profiles that

1 exhibited elevated turbulence levels. It is thus very likely that the observations captured a rare elevated
2 mixing event during station occupation and the associated elevated vertical fluxes do not represent a
3 longer-term average.

4 Although, in the study region atmospheric fluxes of dFe were enhanced relative to global averages
5 (Mahowald et al., 2009) with mean fluxes of 0.63–1.43 $\mu\text{mol m}^{-2} \text{d}^{-1}$, our vertical Fe fluxes from the
6 shallow O_2 depleted waters of 0.95–13.5 $\mu\text{mol m}^{-2} \text{d}^{-1}$ exceeded atmospheric fluxes at all stations apart
7 from station 2 (0.16 $\mu\text{mol m}^{-2} \text{d}^{-1}$) furthest offshore and potentially station 9 (0.08 $\mu\text{mol m}^{-2} \text{d}^{-1}$), where
8 no atmospheric fluxes were determined. The weaker influence of atmospheric deposition in this region
9 close to the coast is in accordance with previous studies that demonstrated sediments to be the major
10 contributor to the Fe inventory in the coastal region of the eastern tropical Atlantic, whereas the
11 importance of atmospheric inputs increases further offshore (Milne et al., 2017). It should be noted
12 that there are considerable uncertainties in the flux estimates presented above. Uncertainties in the
13 diffusive flux originate predominately from the elevated variability of turbulence (see Schafstall et al.,
14 2010 for details) and were calculated here using the upper and lower 95% confidence interval of
15 diffusivity measurements. Uncertainties in the vertical advective flux originate from unaccounted for
16 contributions from e.g. the spatial structure of the wind, particularly in the offshore direction, its
17 temporal variability (e.g. Capet et al., 2004; Desbiolles et al. 2014, 2016; Ndoye et al., 2014), and
18 uncertainties in the satellite wind product near the coast (e.g. Verhoef et al, 2012), and were accounted
19 for by using an estimated error of 50% for the upwelling velocity. Furthermore, the distribution of
20 vertical velocities with depth is assumed to be linear here.

21 Dissolved Co fluxes ranged between 2 and 113 $\text{nmol m}^{-2} \text{d}^{-1}$. These values are lower than reported
22 upwelling fluxes of dCo of 250 $\text{nmol m}^{-2} \text{d}^{-1}$ for this region (Noble et al., 2017), but are larger than
23 atmospheric deposition fluxes of 1.7 $\text{nmol m}^{-2} \text{d}^{-1}$ (Shelley et al., 2015). Fluxes of dMn are downwards
24 from surface waters to O_2 depleted waters due to higher concentrations in surface waters.

25 **3.5 Removal mechanisms and particle interactions**

26 Particles in the water column can either comprise a source or a sink of dissolved TMs. In the top 50 m
27 of the water column a large part of the LpTMs may be part of living biological cells (e.g.
28 phytoplankton) or organic detritus, and can enter the dissolved TM pool by remineralization (Bruland
29 and Lohan, 2006). Additionally, LpTMs may be part of lithogenic phases from Saharan dust and
30 sediment particles, or authigenic phases. Authigenic phases are formed in-situ by TM adsorption onto
31 particle surfaces or by the formation of amorphous TM oxides and hydroxides (e.g. $\text{FeO}(\text{OH})$ in the
32 mineral structure of goethite) (Sherrell and Boyle, 1992), processes referred to as scavenging. The
33 extent of scavenging processes is largely influenced by the amount and type of particles present
34 (Balistrieri et al., 1981; Honeyman et al., 1988).

1 Iron was mainly present in the size fraction $>0.2 \mu\text{m}$ with TDFe concentrations being 0.44–44.5 times
2 higher than dFe ($<0.2 \mu\text{m}$) (Fig. 6a). To investigate the influence of particle load on the distribution
3 between dissolved and particulate phases, the fraction of Lp (Lp/TD) TMs and Lp concentrations are
4 plotted against turbidity for Fe, Co and Mn (Fig. 6b, c). A low fraction of LpFe of around 60% was
5 observed at lowest turbidity. As turbidity increases from 0.1 to 0.2 NTU, the LpFe fraction increased
6 to $>90\%$. This suggests that the fraction of LpFe is tightly coupled to the particle load. Iron adsorption
7 onto particles has been demonstrated to be reversible with a constant exchange between dissolved and
8 particulate fractions (Abadie et al., 2017; Fitzsimmons et al., 2017; John and Adkins, 2012; Labatut et
9 al., 2014). Furthermore, offshore transport of acid-labile Fe particles formed by scavenging
10 (oxidation/adsorption) of dissolved Fe originating from a benthic source was observed in the North
11 Pacific (Lam and Bishop, 2008) and may contribute to the bioavailable Fe pool. Therefore an
12 important fraction of Fe may be transported offshore adsorbed to particles and can enter the dissolved
13 pool by cycling between dissolved and particulate phases.

14 The LpCo fraction ranged between 0 and 75%, and the fraction and concentration of LpCo, showed
15 linear increases with turbidity, indicating an influence of particle load on Co size fractionation, similar
16 to Fe. In contrast to Fe and Co, the fraction of LpMn varied between 3 and 40%, and did not show a
17 correlation with turbidity, whereas LpMn concentrations showed an increase with turbidity. This
18 indicates that an increased presence of particles coincided with enhanced LpMn levels, but that the
19 particle load did not substantially influence the distribution between dMn and LpMn phases and
20 particles therefore did not contribute to the dMn fraction. This suggests that particles did not play a
21 major role in transport of dMn, which agrees with a study on hydrothermal vent plumes, where the
22 distribution of the dMn plume was decoupled from the distribution of the particulate Mn plume
23 (Fitzsimmons et al., 2017).

24 The increase in LpFe concentrations with increasing turbidity was weaker in the surface waters
25 compared to water depths below 50 m (Fig. 6c). This suggests a large additional LpFe source at depth
26 with either a higher Fe content of particles or the presence of different sizes of particles causing
27 different responses in turbidity measurements. The large additional LpFe source at depth is likely
28 associated with benthic dFe inputs, with a subsequent transfer to the particulate phase by scavenging.
29 Enhanced turbidity at depth may also indicate sediment resuspension, which would result in the
30 release of TM-containing particles from sediments and enhanced release of dTMs from sediment pore
31 water. The effect of sediment resuspension is discussed in more detail below (section 3.6.2).

32 In contrast to Fe, the increase in LpCo and LpMn concentrations with turbidity was similar in surface
33 waters and below and suggests less variability in the composition of the particulate Co and Mn phase
34 throughout the water column with a potentially weaker influence of sediment release on the
35 distribution of particulate Mn and Co. A weaker influence of sediment release might be influenced by
36 a weaker release of Co and Mn from sediments in the dissolved form and slower oxidation rates

1 compared to Fe, in particular for Co (Noble et al., 2012), resulting in a slower conversion into the
2 particulate phase. Such an interpretation based on turbidity data alone, however, is very hypothetical
3 and would require further investigation of particulate TM species composition in this area.

4 **3.6 Temporal variability in redox-sensitive trace metals**

5 Large temporal changes in O₂, turbidity and redox-sensitive TMs were observed within a short time
6 scale of a few days at two repeat stations, station 3A/3B and station 8A/8B (Fig. 7 and Fig. S5).

7 Station 3 and 8 were sampled twice with a period of nine days between both deployments for station 3
8 (Fig. 7a) and two days for station 8 (Fig. 7b). At station 3, O₂ concentrations in the upper 50 m were
9 very similar between both deployments, whereas below 50 m O₂ increased from 30 μmol kg⁻¹ during
10 the first deployment to 50 μmol kg⁻¹ nine days later. At the same time, turbidity below 50 m had
11 decreased from 0.35 to below 0.2, and dFe concentrations from a maximum of 10 nmol L⁻¹ to
12 5 nmol L⁻¹ nine days later. In addition, dMn and dCo concentrations decreased from 5 to 3 nmol L⁻¹
13 and 0.14 to 0.12 nmol L⁻¹, respectively. Particularly large changes were also observed for LpTM
14 concentrations with a decrease from 147–322 nmol L⁻¹ to 31–51 nmol L⁻¹ for LpFe, from 0.066–
15 0.114 nmol L⁻¹ to 0.015–0.031 nmol L⁻¹ for LpCo and from 1.24–2.64 to 0.16–0.54 for LpMn. In
16 contrast, no changes in temperature and salinity of the water parcel occurred below 50 m (Fig. 7a).
17 Similar changes in O₂ and turbidity were observed at station 8. During the first deployment a local
18 minimum in O₂ below 30 μmol kg⁻¹ was present between 105 m and 120 m water depths which
19 coincided with a maximum in turbidity of 0.4 (Fig. 7b). In contrast O₂ concentrations and turbidity
20 during the second deployment were relatively constant (50–60 μmol kg⁻¹ O₂ and turbidity 0.2) below
21 50 m. At the depth of the local O₂ minimum and turbidity maximum, concentrations of dFe, dMn and
22 dCo were elevated during the first deployment with concentrations of 9.4 ± 2.1 nmol dFe L⁻¹,
23 3.7 ± 0.6 nmol dMn L⁻¹ and 0.145 ± 0.033 nmol dCo L⁻¹ in comparison to 4.6 ± 1.0 nmol dFe L⁻¹,
24 2.6 ± 0.5 nmol dMn L⁻¹, and 0.122 ± 0.028 nmol dCo L⁻¹ at similar depth during the second
25 deployment.

26 *3.6.1 Remineralization*

27 We compared the results of the redox-sensitive TMs to other nutrient-like TMs and PO₄. For both
28 repeat stations only small changes in dCd (Stn 3A: 0.107–0.231 nmol L⁻¹; Stn 3B: 0.135–
29 0.150 nmol L⁻¹) and PO₄ (Stn 3A: 1.59–1.85 μmol L⁻¹; Stn 3B: 1.55–1.71 μmol L⁻¹) concentrations
30 were observed below 50 m (Fig. 8), suggesting that only a small fraction of dFe under lower O₂
31 conditions was supplied by more intense remineralization of biogenic particles in the water column.

32 A weak influence of remineralization processes on the variability in dFe concentrations was confirmed
33 by substantially higher dFe/C ratios at lower O₂ concentrations (40–72 μmol mol⁻¹ at Stn 3A compared
34 to 33–41 μmol mol⁻¹ at Stn 3B, both below 50 m water depth). Assuming a dFe/C ratio of around 12

1 (see section 3.4.1) from remineralization, only about 0.25 nmol L^{-1} of the difference in dFe
2 concentrations between repeated deployments can be explained by the difference in remineralization,
3 suggesting that most of the difference in dFe between deployments was caused by changes in source
4 inputs, such as enhanced sediment release during lower bottom water O_2 concentrations, or slower
5 removal by oxidation under lower O_2 conditions.

6 In contrast, dCo/C ratios were similar between repeat deployments within the OMZ ($0.90\text{--}1.04$ at Stn
7 3A and $0.92\text{--}1.06 \mu\text{mol mol}^{-1}$ at Stn 3B). Thus, remineralization could be a reason for the changes in
8 observed dCo concentrations during repeated deployments. This is in accordance with previously
9 observed correlation of dCo with PO_4^{3-} in addition to O_2 (Baars and Croot, 2015; Saito et al., 2017).
10 However, we observed a very low Pearson correlation of dCo with PO_4 of only 0.15 compared to
11 oxygen (-0.58) (Supplementary Table S1) below 50 m water depth, suggesting a stronger influence of
12 oxygen than remineralization on the overall distribution of dCo for our study area.

13 Similar to Fe, higher dMn/C ratios were observed at lower O_2 concentrations ($3.4\text{--}5.5 \mu\text{mol mol}^{-1}$ at
14 Stn 3A compared to $2.1\text{--}2.9 \mu\text{mol mol}^{-1}$ at Stn 3B). These results indicate that processes other than
15 remineralization are also important for the change in dMn concentrations. An additional factor
16 compared to Fe, might involve changes in intensity of photoreduction which may be influenced by
17 differences in surface turbidity observed at station 3 (lower dMn/C and higher surface turbidity during
18 second deployment). This, however, cannot explain the changes in dMn/C at station 8, where a higher
19 surface turbidity coincided with a higher dMn/C ratio at the local minimum in O_2 .

20 *3.6.2 Atmospheric dust deposition and sediment resuspension*

21 Within the OMZ at station 3 and 8, dAl concentrations ranged between 10 and 15 nmol L^{-1} , and LpAl
22 concentration between 1.2 and 11.1 nmol L^{-1} and no substantial changes were observed between
23 deployments (Fig. 8). As lithogenic material has a high Al content, no substantial changes in Al
24 concentrations signify that lithogenic inputs did not differ greatly between the deployments.
25 Consequently neither increased atmospheric input, nor sediment resuspension are likely to explain the
26 differences in turbidity and redox-sensitive TM concentrations. Hence, changes in turbidity may
27 mainly have been caused by biogenic particles, such as resuspended organic matter (Thomsen et al.,
28 2019). This finding can be confirmed by substantial changes in TM/Al ratios observed during the
29 deployments (Table 2 and Fig. S6). The Fe/Al ratios in the solid phase of underlying sediments during
30 the cruise were $0.23\text{--}0.30$ (Schroller-Lomnitz et al., 2018) with Mn/Al ratios of $0.0015\text{--}0.0020$
31 (Schroller-Lomnitz, pers. com.). Slight increases in LpAl towards the sediment indicate some
32 influence of sediment resuspension on the TM distribution. Overall much higher TM/Al ratios
33 compared to ratios in the sediments and aerosol samples from this region (Fe/Al: 0.37 ± 0.02 , Co/Al:
34 0.00016 ± 0.00002 , Mn/Al: 0.0061 ± 0.0002 ; Shelley et al., 2015), suggest a large additional source of
35 Fe, Co and Mn in the OMZ close to the shelf. This again points towards a large influence of benthic

1 release of Fe, Co and Mn from sediment pore waters and subsequent partial adsorption to particle
2 surfaces.

3 *3.6.3 Other possible causes for TM variability*

4 From the comparison above, we can conclude that the variations in Fe concentrations during repeated
5 deployments were not caused by increased remineralization or changes in lithogenic inputs from
6 atmospheric deposition or sediment resuspension. The large changes in the Lp fractions must therefore
7 be of biogenic or authigenic origin. If all LpCo would be present in biogenic particles of suspended
8 phytoplankton cells, at our observed maximum of 0.114 nmol L⁻¹ LpCo at station 3A we would expect
9 around 4.6 nmol L⁻¹ LpFe in sinking phytoplankton, using an average Fe/Co ratio in phytoplankton of
10 40 (Moore et al., 2013) (observed ratios close to our study area were 20–40; Twining et al., 2015).
11 However, LpFe concentrations were 322 nmol L⁻¹ and thereby 70 times larger than our estimate in
12 biogenic particles (4.6 nmol L⁻¹), revealing that the majority of LpFe must be authigenically formed.
13 Altogether our results suggest that changes in particle load as indicated by changes in turbidity do not
14 comprise a major source of dFe, moreover a sink of previously dissolved Fe. Therefore, higher
15 dissolved and Lp concentrations during the first deployment with lower O₂ concentrations must be
16 caused by a stronger benthic source of dissolved Fe.

17 It is not possible to extract from our data whether the stronger benthic source under low O₂ conditions
18 is directly driven by lower O₂ concentrations in surface sediments and in the water column resulting in
19 higher benthic Fe fluxes and slower oxidation rates in the water column, or by a longer residence time
20 of the water mass on the shelf. However, increased benthic fluxes are in accordance with previous
21 findings from ex-situ sediment incubation experiments, where Fe fluxes increased with decreasing O₂
22 concentrations (Homoky et al., 2012). Therefore, we hypothesize that with a reduction of bottom water
23 O₂ concentrations from 50 to 30 μmol kg⁻¹, drastically more Fe is effectively released from the
24 sediments by diminished oxidation rates at the sediment-water interface, and that a large fraction gets
25 directly adsorbed onto particles. Therefore, particles do not compose a major source of Fe here, but
26 may play an important role in Fe offshore transport.

27 Due to much lower changes in concentrations of dissolved and LpCo, and the additional effect of
28 photoreduction and strong scavenging for Mn, we were unable to resolve the main mechanisms for
29 changes in Co and Mn concentrations with changes in O₂ and turbidity. Nevertheless, due to their
30 similar redox-sensitive behavior and distribution in OMZs, it is likely that they are also affected by
31 reduced O₂ conditions. The magnitude of response however, is much lower.

32 **4. CONCLUSION**

33 Sediments are an important source of Fe, Co and Mn to OMZ waters in the Mauritanian shelf region.
34 Remineralization and atmospheric deposition appear less important than benthic sources for dFe, with

1 vertical fluxes exceeding atmospheric fluxes but gaining importance with distance from shelf.
2 However, deposition of atmospheric dust is a source of Fe to sediments in our study region and
3 consequently indirectly contributes to benthic released TMs. We showed that changes in O₂
4 concentrations from 30 to 50 μmol kg⁻¹ had a substantial influence on dissolved and LpFe
5 concentrations and to a lesser extent on Co and Mn concentrations by decreasing the sediment source
6 strength. The presence of a large part of sediment-derived Fe in the leachable particulate phase
7 highlights the importance of offshore particle transport on the Fe inventory, including the dissolved
8 form by reversible scavenging. To our knowledge, this is the first field study that demonstrated strong
9 short-term variability in redox-sensitive TMs over a few days to be directly linked to changes in O₂.
10 These findings demonstrate that projected long-term changes in oceanic O₂ concentrations will impact
11 biogeochemical cycles and have important implications for global TM distributions and their process
12 parameterisations in biogeochemical models. Current models do not account for small changes in O₂
13 on TM distributions and benthic TM fluxes. Determining the processes involved and quantifying the
14 effect of O₂ will be crucial for the implementation into current modeling approaches. Not all processes
15 could be resolved in this study, including the influence of the residence time of the water masses on
16 the shelf compared to the direct influence of O₂, and it is unclear whether the changes observed on a
17 small scale are readily transferable to a global scale. Therefore, we suggest further investigations on
18 short-term variability of O₂ and particle load in the Mauritanian and other dynamic OMZs including
19 water column TM measurement in combination with benthic TM fluxes and more detailed analysis of
20 amount and types/composition of present particles.

21

22 *Data availability.* The CTD sensor and nutrient bottle data are freely available at
23 <https://doi.pangaea.de/10.1594/PANGAEA.860480> and
24 <https://doi.pangaea.de/10.1594/PANGAEA.885109> respectively. According to the SFB754 data policy
25 (<https://www.sfb754.de/de/data>, all remaining data (trace metal data set) associated with this
26 manuscript will be published at PANGAEA (www.pangaea.de, search projects:sfb754) upon publication
27 of this manuscript.

28 *Author contributions.* IR analyzed the trace metal concentrations and drafted the manuscript. EPA and
29 MG designed the project and CS carried out the trace metal sampling at sea. J-LMB oversaw, and BW
30 carried out, the aluminium sample analysis. MD carried out the microstructure measurements at sea,
31 oversaw the calculation of the vertical flux estimates and contributed to the writing of the manuscript.
32 JL carried out the processing of microstructure data and calculation of the eddy diffusivity. JS, BG and
33 PR carried out the radium isotope analysis and their interpretation. IR and MG oversaw, and Fabian
34 Wolf carried out, the iodide analysis. All co-authors commented on the manuscript.

35 *Competing interests.* The authors declare that they have no conflict of interest.

1 *Acknowledgements.* The authors would like to thank the captain and the crew from RV Meteor and
2 chief scientist Dr. Stefan Sommer from the M107 cruise. This work was funded by the Deutsche
3 Forschungsgemeinschaft as part of Sonderforschungsbereich (SFB) 754: 'Climate-Biogeochemistry
4 Interactions in the Tropical Ocean'. Fabian Wolf is thanked for carrying out the analysis of iodide and
5 Peter Streu for help with the general lab work. The International Atomic Energy Agency is grateful to
6 the Government of the Principality of Monaco for the support provided to its Environment
7 Laboratories. Analyses and visualizations of aerosol optical depth (Supplementary Material) were
8 produced with the Giovanni online data system, developed and maintained by the NASA GES DISC.

9 REFERENCES

- 10 Abadie, C., Lacan, F., Radic, A., Pradoux, C., and Poitrasson, F.: Iron isotopes reveal distinct
11 dissolved iron sources and pathways in the intermediate versus deep Southern Ocean, *P Natl*
12 *Acad Sci USA*, 114, 858-863, <https://doi.org/10.1073/pnas.1603107114>, 2017.
- 13 Achterberg, E. P., Steigenberger, S., Marsay, C. M., LeMoigne, F. A. C., Painter, S. C., Baker, A. R.,
14 Connelly, D. P., Moore, C. M., Tagliabue, A., and Tanhua, T.: Iron Biogeochemistry in the
15 High Latitude North Atlantic Ocean, *Sci Rep*, 8, <https://doi.org/10.1038/s41598-018-19472-1>,
16 2018.
- 17 Baars, O., and Croot, P. L.: Dissolved cobalt speciation and reactivity in the eastern tropical North
18 Atlantic, *Mar. Chem.*, 173, 310-319, <https://doi.org/10.1016/j.marchem.2014.10.006>, 2015.
- 19 Baker, A. R., Adams, C., Bell, T. G., Jickells, T. D., and Ganzeveld, L.: Estimation of atmospheric
20 nutrient inputs to the Atlantic Ocean from 50°N to 50°S based on large-scale field sampling:
21 Iron and other dust-associated elements, *Global Biogeochem Cy*, 27, 755-767,
22 <https://doi.org/10.1002/gbc.20062>, 2013.
- 23 Balistrieri, L., Brewer, P. G., and Murray, J. W.: Scavenging residence times of trace metals and
24 surface chemistry of sinking particles in the deep ocean, *Deep Sea Res Part A. Oceanogr Res*
25 *Pap*, 28(2), 101-121, [https://doi.org/10.1016/0198-0149\(81\)90085-6](https://doi.org/10.1016/0198-0149(81)90085-6), 1981. Barton, E. D.: The
26 Poleward Undercurrent On The Eastern Boundary Of The Subtropical North Atlantic. In:
27 Poleward Flows Along Eastern Ocean Boundaries, Neshyba, S. J., Mooers, C. N. K., Smith, R.
28 L., and Barber, R. T. (Eds.), Springer-Verlag, New York,
29 <https://doi.org/10.1029/CE034p0082>, 1989.
- 30 Barton, E. D., Aristegui, J., Tett, P., Canton, M., Garcia-Braun, J., Hernandez-Leon, S., Nykjaer, L.,
31 Almeida, C., Almunia, J., Ballesteros, S., Basterretxea, G., Escanez, J., Garcia-Weill, L.,
32 Hernandez-Guerra, A., Lopez-Laatzén, F., Molina, R., Montero, M. F., Navarro-Perez, E.,
33 Rodriguez, J. M., van Lenning, K., Velez, H., and Wild, K.: The transition zone of the Canary
34 Current upwelling region, *Prog Oceanogr*, 41, 455-504, [https://doi.org/10.1016/S0079-](https://doi.org/10.1016/S0079-6611(98)00023-8)
35 [6611\(98\)00023-8](https://doi.org/10.1016/S0079-6611(98)00023-8), 1998.

1 Beck, A. J., Tsukamoto, Y., Tovar-Sanchez, A., Huerta-Diaz, M., Bokuniewicz, H. J., and Sanudo-
2 Wilhelmy, S. A.: Importance of geochemical transformations in determining submarine
3 groundwater discharge-derived trace metal and nutrient fluxes, *Appl Geochem*, 22, 477-490,
4 [https://doi.org/ 10.1016/j.apgeochem.2006.10.005](https://doi.org/10.1016/j.apgeochem.2006.10.005), 2007.

5 Biller, D. V. and Bruland, K. W.: Sources and distributions of Mn, Fe, Co, Ni, Cu, Zn, and Cd relative
6 to macronutrients along the central California coast during the spring and summer upwelling
7 season, *Mar Chem*, 155, 50-70, [https://doi.org/ 10.1016/j.marchem.2013.06.003](https://doi.org/10.1016/j.marchem.2013.06.003), 2013.

8 Boyd, P. W.: Biogeochemistry - Iron findings, *Nature*, 446, 989-991, [https://doi.org/
9 10.1038/446989a](https://doi.org/10.1038/446989a), 2007.

10 Boyle, E. A., Lee, J.-M., Echevoyen, Y., Noble, A., Moos, S., Carrasco, G., Zhao, N., Kayser, R.,
11 Zhang, J., and Gamo, T.: Anthropogenic lead emissions in the ocean: The evolving global
12 experiment, *Oceanography*, 27, 69-75, <https://doi.org/10.5670/oceanog.2014.10>, 2014.

13 Brandt, P., Bange, H. W., Banyte, D., Dengler, M., Didwischus, S. H., Fischer, T., Greatbatch, R. J.,
14 Hahn, J., Kanzow, T., Karstensen, J., Krortzinger, A., Krahnmann, G., Schmidtko, S., Stramma,
15 L., Tanhua, T., and Visbeck, M.: On the role of circulation and mixing in the ventilation of
16 oxygen minimum zones with a focus on the eastern tropical North Atlantic, *Biogeosciences*,
17 12, 489-512, <https://doi.org/10.5194/bg-12-489-2015>, 2015.

18 Bridgestock, L., van de Flierdt, T. V., Rehkamper, M., Paul, M., Middag, R., Milne, A., Lohan, M. C.,
19 Baker, A. R., Chance, R., Khondoker, R., Strekopytov, S., Humphreys-Williams, E.,
20 Achterberg, E. P., Rijkenberg, M. J. A., Gerringa, L. J. A., and de Baar, H. J. W.: Return of
21 naturally sourced Pb to Atlantic surface waters, *Nat Commun*, 7, 12921,
22 <https://doi.org/10.1038/ncomms12921>, 2016.

23 Browning, T. J., Achterberg, E. P., Rapp, I., Engel, A., Bertrand, E. M., Tagliabue, A., and Moore, C.
24 M.: Nutrient co-limitation at the boundary of an oceanic gyre, *Nature*, 551, 242-246,
25 <https://doi.org/10.1038/nature24063>, 2017.

26 Bruland, K. W. and Lohan, M. C.: Controls of Trace Metals in Seawater. In: *The Oceans and Marine
27 Geochemistry*, Elderfield, H. (Ed.), Treatise on Geochemistry, 6, Elsevier, Oxford, 2006.

28 Buck, C. S., Landing, W. M., Resing, J. A., and Measures, C. I.: The solubility and deposition of
29 aerosol Fe and other trace elements in the North Atlantic Ocean: Observations from the A16N
30 CLIVAR/CO₂ repeat hydrography section, *Mar Chem*, 120, 57-70,
31 <https://doi.org/10.1016/j.marchem.2008.08.003>, 2010.

32 Burdige, D. J.: The biogeochemistry of manganese and iron reduction in marine sediments, *Earth-Sci
33 Rev*, 35, 249-284, [https://doi.org/10.1016/0012-8252\(93\)90040-E](https://doi.org/10.1016/0012-8252(93)90040-E), 1993.

34 Capet, X. J., Marchesiello, P., and McWilliams, J. C.: Upwelling response to coastal wind profiles,
35 *Geophys Res Lett*, 31, L13311, <https://doi.org/10.1029/2004GL020123>, 2004.

1 Chaillou, G., Anschutz, P., Lavaux, G., Schafer, J., and Blanc, G.: The distribution of Mo, U, and Cd
2 in relation to major redox species in muddy sediments of the Bay of Biscay, *Mar Chem*, 80,
3 41-59, [https://doi.org/10.1016/S0304-4203\(02\)00097-X](https://doi.org/10.1016/S0304-4203(02)00097-X), 2002.

4 Charette, M. A., Morris, P. J., Henderson, P. B., and Moore, W. S.: Radium isotope distributions
5 during the US GEOTRACES North Atlantic cruises, *Mar Chem*, 177, 184-195,
6 <https://doi.org/10.1016/j.marchem.2015.01.001>, 2015.

7 Conway, T. M. and John, S. G.: Quantification of dissolved iron sources to the North Atlantic Ocean,
8 *Nature*, 511, 212-215, <https://doi.org/10.1038/nature13482>, 2014.

9 Croot, P. L., Streu, P., and Baker, A. R.: Short residence time for iron in surface seawater impacted by
10 atmospheric dry deposition from Saharan dust events, *Geophys Res Lett*, 31(23),
11 <https://doi.org/10.1029/2004GL020153>, 2004.

12 Cyr, F., Bourgault, D., Galbraith, P. S., and Gosselin, M.: Turbulent nitrate fluxes in the Lower St.
13 Lawrence Estuary, Canada, *J Geophys Res-Oceans*, 120, 2308-2330,
14 <https://doi.org/10.1002/2014jc010272>, 2015.

15 Dale, A.W., Sommer, S., Ryabenko, E., Noffke, A., Bohlen, L., Wallmann, K., Stolpovsky, K.,
16 Greinert, J. and Pfannkuche, O.: Benthic nitrogen fluxes and fractionation of nitrate in the
17 Mauritanian oxygen minimum zone (Eastern Tropical North Atlantic), *Geochim Cosmochim*
18 *Acta*, 134 (0), 234–256, <https://doi.org/10.1016/j.gca.2014.02.026>, 2014.

19 Dammshäuser, A., Wagener, T., and Croot, P. L.: Surface water dissolved aluminum and titanium:
20 Tracers for specific time scales of dust deposition to the Atlantic?, *Geophys Res Lett*, 38,
21 L24601, <https://doi.org/10.1029/2011gl049847>, 2011.

22 Desbiolles, F., Blanke, B., and Bentamy, A.: Short-term upwelling events at the western African coast
23 related to synoptic atmospheric structures as derived from satellite observations, *J Geophys*
24 *Res-Oceans*, 119, 461-483, <https://doi.org/10.1002/2013JC009278>, 2014.

25 Desbiolles, F., Blanke, B., Bentamy, A., and Roy, C.: Response of the Southern Benguela upwelling
26 system to fine-scale modifications of the coastal wind, *J Mar Syst*, 156, 46-55,
27 <https://doi.org/10.1016/j.jmarsys.2015.12.002>, 2016.

28 Elrod, V. A., Berelson, W. M., Coale, K. H., and Johnson, K. S.: The flux of iron from continental
29 shelf sediments: A missing source for global budgets, *Geophys Res Lett*, 31, L12307,
30 <https://doi.org/10.1029/2004gl020216>, 2004.

31 Eriksen, C. C.: Observations of internal wave reflection off sloping bottoms, *J Geophys Res-Oceans*,
32 87, 525-538, <https://doi.org/10.1029/JC087iC01p00525>, 1982.

33 Fairall, C.W., Bradley, E.F., Hare, J.E., Grachev, A.A., and Edson, J.B.: Bulk Parameterization of
34 Air–Sea Fluxes: Updates and Verification for the COARE Algorithm, *J Climate*, 16, 571–591,
35 [https://doi.org/10.1175/1520-0442\(2003\)016<0571:BPOASF>2.0.CO;2](https://doi.org/10.1175/1520-0442(2003)016<0571:BPOASF>2.0.CO;2), 2003.

36 Fitzsimmons, J. N., Zhang, R. F., and Boyle, E. A.: Dissolved iron in the tropical North Atlantic
37 Ocean, *Mar Chem*, 154, 87-99, <https://doi.org/10.1016/j.marchem.2013.05.009>, 2013.

1 Fitzsimmons, J. N., John, S. G., Marsay, C. M., Hoffman, C. L., Nicholas, S. L., Toner, B. M.,
2 German, C. R., and Sherrell, R. M.: Iron persistence in a distal hydrothermal plume supported
3 by dissolved-particulate exchange, *Nat Geosci*, 10, 195-201,
4 <https://doi.org/10.1038/Ngeo2900>, 2017.

5 Froelich, P. N., Klinkhammer, G. P., Bender, M. L., Luedtke, N. A., Heath, G. R., Cullen, D.,
6 Dauphin, P., Hammond, D., Hartman, B., and Maynard, V.: Early oxidation of organic matter
7 in pelagic sediments of the Eastern Equatorial Atlantic: suboxic diagenesis, *Geochim*
8 *Cosmochim Ac*, 43, 1075-1090, [https://doi.org/10.1016/0016-7037\(79\)90095-4](https://doi.org/10.1016/0016-7037(79)90095-4), 1979.

9 Garcia-Solsona, E., Garcia-Orellana, J., Masqué, P., and Dulaiova, H.: Uncertainties associated with
10 ^{223}Ra and ^{224}Ra measurements in water via a Delayed Coincidence Counter (RaDeCC), *Mar*
11 *Chem*, 109, 198-219, <https://doi.org/10.1016/j.marchem.2007.11.006>, 2008.

12 Gehlen, M., Beck, L., Calas, G., Flank, A. M., Van Bennekom, A. J., and Van Beusekom, J. E. E.:
13 Unraveling the atomic structure of biogenic silica: Evidence of the structural association of Al
14 and Si in diatom frustules, *Geochim Cosmochim Ac*, 66, 1601-1609,
15 [https://doi.org/10.1016/S0016-7037\(01\)00877-8](https://doi.org/10.1016/S0016-7037(01)00877-8), 2002.

16 Gill, A.: *Atmosphere-Ocean Dynamics*, Academic Press, California, 1982.

17 Grasshoff, K., Ehrhardt, M., and Kremling, K.: *Methods of Seawater Analysis*, Verlag Chemie,
18 Weinheim, 1983.

19 Green, M. A., Aller, R. C., Cochran, J. K., Lee, C., and Aller, J. Y.: Bioturbation in shelf/slope
20 sediments off Cape Hatteras, North Carolina: the use of ^{234}Th , Chl-*a*, and Br^- to evaluate rates
21 of particle and solute transport, *Deep-Sea Res Pt II*, 49, 4627-4644,
22 [https://doi.org/10.1016/S0967-0645\(02\)00132-7](https://doi.org/10.1016/S0967-0645(02)00132-7), 2002.

23 Hahn, J., Brandt, P., Schmidtko, S., and Krahnmann, G.: Decadal oxygen change in the eastern tropical
24 North Atlantic, *Ocean Sci*, 13, 551-576, <https://doi.org/10.5194/os-13-551-2017>, 2017.

25 Hansen, H. P.: Determination of oxygen, *Methods of Seawater Analysis*, Third Edition, 2007. 75-89,
26 2007.

27 Hartmann, M., Müller, P.J., Suess, E., and van der Weijden, C.H.: Chemistry of Late Quaternary
28 sediments and their interstitial waters of sediment cores from the North-West African
29 continental margin, in Supplement to: Hartmann, M et al. (1976): Chemistry of Late
30 Quaternary sediments and their interstitial waters from the northwest African continental
31 margin. Meteor Forschungsergebnisse, Deutsche Forschungsgemeinschaft, Reihe C Geologie
32 und Geophysik, Gebrüder Bornträger, Berlin, Stuttgart, C24, 1-67, edited, PANGAEA, 1976.

33 Hatta, M., Measures, C. I., Wu, J. F., Roshan, S., Fitzsimmons, J. N., Sedwick, P., and Morton, P.: An
34 overview of dissolved Fe and Mn distributions during the 2010-2011 US GEOTRACES north
35 Atlantic cruises: GEOTRACES GA03, *Deep-Sea Res Pt II*, 116, 117-129,
36 <https://doi.org/10.1016/j.dsr2.2014.07.005>, 2015.

1 Hayes, S. P., Chang, P., and McPhaden, M. J.: Variability of the sea surface temperature in the eastern
2 equatorial Pacific during 1986–1988, *J Geophys Res*, 96, 10553-10566,
3 <https://doi.org/10.1029/91JC00942>, 1991.

4 Hawco, N. J., Ohnemus, D. C., Resing, J. A., Twining, B. S., and Saito, M. A.: A dissolved cobalt
5 plume in the oxygen minimum zone of the eastern tropical South Pacific, *Biogeosciences*, 13,
6 5697-5717, <https://doi.org/10.5194/bg-13-5697-2016>, 2016.

7 Heggie, D. T.: Copper in Surface Waters of the Bering Sea, *Geochim Cosmochim Acta*, 46, 1301-1306,
8 [https://doi.org/10.1016/0016-7037\(82\)90014-X](https://doi.org/10.1016/0016-7037(82)90014-X), 1982.

9 Helly, J. J. and Levin, L. A.: Global distribution of naturally occurring marine hypoxia on continental
10 margins, *Deep-Sea Res Pt I*, 51, 1159-1168, <https://doi.org/10.1016/j.dsr.2004.03.009>, 2004.

11 Henderson, P., Morris, P., Moore, W., and Charette, M.: Methodological advances for measuring low-
12 level radium isotopes in seawater, *J Radioanal Nucl Ch*, 296, 357-362,
13 <https://doi.org/10.1007/s10967-012-2047-9>, 2013.

14 Homoky, W. B., Severmann, S., McManus, J., Berelson, W. M., Riedel, T. E., Statham, P. J., and
15 Mills, R. A.: Dissolved oxygen and suspended particles regulate the benthic flux of iron from
16 continental margins, *Mar Chem*, 134, 59-70, <https://doi.org/10.1016/j.marchem.2012.03.003>,
17 2012.

18 Homoky, W. B., Weber, T., Berelson, W. M., Conway, T. M., Henderson, G. M., van Hulten, M.,
19 Jeandel, C., Severmann, S., and Tagliabue, A.: Quantifying trace element and isotope fluxes at
20 the ocean-sediment boundary: a review, *Philos T R Soc A*, 374, 20160246,
21 <https://doi.org/10.1098/rsta.2016.0246>, 2016.

22 Honeyman, B. D., Balistrieri, L. S., and Murray, J. W.: Oceanic trace metal scavenging: the
23 importance of particle concentration. *Deep Sea Res Part A. Oceanogr Res Pap*, 35(2), 227-
24 246, [https://doi.org/10.1016/0198-0149\(88\)90038-6](https://doi.org/10.1016/0198-0149(88)90038-6), 1988.

25 Hurst, M. P., Aguilar-Islas, A. M., and Bruland, K. W.: Iron in the southeastern Bering Sea: Elevated
26 leachable particulate Fe in shelf bottom waters as an important source for surface waters, *Cont
27 Shelf Res*, 30, 467-480, <https://doi.org/10.1016/j.csr.2010.01.001>, 2010.

28 Hydes, D. J. and Liss, P. S.: Fluorimetric method for determination of low concentrations of dissolved
29 aluminum in natural waters, *Analyst*, 101, 922-931, <https://doi.org/10.1039/an9760100922>,
30 1976.

31 Jickells, T. D.: The inputs of dust derived elements to the Sargasso Sea; a synthesis, *Mar Chem*, 68(1-
32 2), 5-14, [https://doi.org/10.1016/S0304-4203\(99\)00061-4](https://doi.org/10.1016/S0304-4203(99)00061-4), 1999.

33 John, S. G. and Adkins, J.: The vertical distribution of iron stable isotopes in the North Atlantic near
34 Bermuda, *Global Biogeochem Cy*, 26, GB2034, <https://doi.org/10.1029/2011gb004043>, 2012.

35 Johnson, K. S., Stout, P. M., Berelson, W. M., and Sakamotoarnold, C. M.: Cobalt and copper
36 distributions in the waters of Santa-Monica Basin, California, *Nature*, 332, 527-530,
37 <https://doi.org/10.1038/332527a0>, 1988.

1 Kagaya, S., Maeba, E., Inoue, Y., Kamichatani, W., Kajiwara, T., Yanai, H., Saito, M., and Tohda, K.:
2 A solid phase extraction using a chelate resin immobilizing carboxymethylated
3 pentaethylenhexamine for separation and preconcentration of trace elements in water
4 samples, *Talanta*, 79, 146-152, <https://doi.org/10.1016/j.talanta.2009.03.016>, 2009.

5 Karstensen, J., Stramma, L., and Visbeck, M.: Oxygen minimum zones in the eastern tropical Atlantic
6 and Pacific oceans, *Prog Oceanogr*, 77, 331-350,
7 <https://doi.org/10.1016/j.pocean.2007.05.009>, 2008.

8 Klenz, T., Dengler, M., and Brandt, P.: Seasonal variability of the Mauritanian Undercurrent and
9 Hydrography at 18°N, *J Geophys Res: Oceans*, 123, 8122-8137,
10 <https://doi.org/10.1029/2018JC014264>, 2018.

11 Kock, A., Schafstall, J., Dengler, M., Brandt, P., and Bange, H. W.: Sea-to-air and diapycnal nitrous
12 oxide fluxes in the eastern tropical North Atlantic Ocean, *Biogeosciences*, 9, 957-964,
13 <https://doi.org/10.5194/bg-9-957-2012>, 2012.

14 Köllner, M., Visbeck, M., Tanhua, T., and Fischer, T.: Diapycnal diffusivity in the core and oxycline
15 of the tropical North Atlantic oxygen minimum zone, *J Marine Syst*, 160, 54-63,
16 <https://doi.org/10.1016/j.jmarsys.2016.03.012>, 2016.

17 Kounta, L., Capet, X., Jouanno, J., Kolodziejczyk, N., Sow, B., and Gaye, A. T.: A model perspective
18 on the dynamics of the shadow zone of the eastern tropical North Atlantic – Part 1: the
19 poleward slope currents along West Africa, *Ocean Sci*, 14, 971-997,
20 <https://doi.org/10.5194/os-14-971-2018>, 2018.

21 Labatut, M., Lacan, F., Pradoux, C., Chmeleff, J., Radic, A., Murray, J. W., Poitrasson, F., Johansen,
22 A. M., and Thil, F.: Iron sources and dissolved-particulate interactions in the seawater of the
23 Western Equatorial Pacific, iron isotope perspectives, *Global Biogeochem Cy*, 28, 1044-1065,
24 <https://doi.org/10.1002/2014gb004928>, 2014.

25 Lam, P. J. and Bishop, J. K. B.: The continental margin is a key source of iron to the HNLC North
26 Pacific Ocean, *Geophys Res Lett*, 35, L07608, <https://doi.org/10.1029/2008gl033294>, 2008.

27 Lam, P. J., Ohnemus, D. C., and Marcus, M. A.: The speciation of marine particulate iron adjacent to
28 active and passive continental margins, *Geochim Cosmochim Acta*, 80, 108-124,
29 <https://doi.org/10.1016/j.gca.2011.11.044>, 2012.

30 Lathuilière, C., Echevin, V., and Lévy, M.: Seasonal and intraseasonal surface chlorophyll-a
31 variability along the northwest African coast, *J Geophys Res*, 113, C05007,
32 <https://doi.org/10.1029/2007JC004433>, 2008.

33 Liu, X. W. and Millero, F. J.: The solubility of iron in seawater, *Mar Chem*, 77, 43-54,
34 [https://doi.org/10.1016/S0304-4203\(01\)00074-3](https://doi.org/10.1016/S0304-4203(01)00074-3), 2002.

35 Lohan, M. C. and Bruland, K. W.: Elevated Fe(II) and dissolved Fe in hypoxic shelf waters off
36 Oregon and Washington: An enhanced source of iron to coastal upwelling regimes, *Environ
37 Sci Technol*, 42, 6462-6468, <https://doi.org/10.1021/es800144j>, 2008.

1 Luther, G. W., Swartz, C. B., and Ullman, W. J.: Direct determination of iodide in seawater by
2 Cathodic Stripping Square-Wave Voltammetry, *Anal Chem*, 60, 1721-1724,
3 <https://doi.org/10.1021/ac00168a017>, 1988.

4 Machu, E., Capet, X., Estrade, P. A., Ndoye, S., Brajard, J., Baurand, F., Auger, P.-A., Lazar, A., and
5 Brehmer, P.: First evidence of anoxia and nitrogen loss in the southern Canary upwelling
6 system, *Geophys Res Lett*, 46, 2619-2627, <https://doi.org/10.1029/2018GL079622>, 2019.

7 Mahowald, N. M., Engelstaedter, S., Luo, C., Sealy, A., Artaxo, P., Benitez-Nelson, C., Bonnet, S.,
8 Chen, Y., Chuang, P. Y., Cohen, D. D., Dulac, F., Herut, B., Johansen, A. M., Kubilay, N.,
9 Losno, R., Maenhaut, W., Paytan, A., Prospero, J. A., Shank, L. M., and Siefert, R. L.:
10 Atmospheric Iron Deposition: Global Distribution, Variability, and Human Perturbations,
11 *Annu Rev Mar Sci*, 1, 245-278, <https://doi.org/10.1146/annurev.marine.010908.163727>, 2009.

12 Martin, J. H., Gordon, R. M., Fitzwater, S., and Broenkow, W. W.: Vertex - Phytoplankton Iron
13 Studies in the Gulf of Alaska, *Deep-Sea Res*, 36, 649-680, <https://doi.org/10.1016/0198->
14 [0149\(89\)90144-1](https://doi.org/10.1016/0198-0149(89)90144-1), 1989.

15 Mawji, E. and Schlitzer, R. and Dodas, E. M. and Abadie, C. and Abouchami, W. and Anderson, R. F.
16 and Baars, O. and Bakker, K. and Baskaran, M. and Bates, N. R. and Bluhm, K. and Bowie,
17 A. and Bown, J. and Boye, M. and Boyle, E. A. and Branellec, P. and Bruland, K. W. and
18 Brzezinski, M. A. and Bucciarelli, E. and Buesseler, K. and Butler, E. and Cai, P. H. and
19 Cardinal, D. and Casciotti, K. and Chaves, J. and Cheng, H. and Chever, F. and Church, T. M.
20 and Colman, A. S. and Conway, T. M. and Croot, P. L. and Cutter, G. A. and de Baar, H. J.
21 W. and de Souza, G. F. and Dehairs, F. and Deng, F. F. and Dieu, H. T. and Dulaquais, G. and
22 Echegoyen-Sanz, Y. and Edwards, R. L. and Fahrbach, E. and Fitzsimmons, J. and Fleisher,
23 M. and Frank, M. and Friedrich, J. and Fripiat, F. and Galer, S. J. G. and Gamo, T. and
24 Solsona, E. G. and Gerringa, L. J. A. and Godoy, J. M. and Gonzalez, S. and Grosstefan, E.
25 and Hatta, M. and Hayes, C. T. and Heller, M. I. and Henderson, G. and Huang, K. F. and
26 Jeandel, C. and Jenkins, W. J. and John, S. and Kenna, T. C. and Klunder, M. and Kretschmer,
27 S. and Kumamoto, Y. and Laan, P. and Labatut, M. and Lacan, F. and Lam, P. J. and
28 Lannuzel, D. and le Moigne, F. and Lechtenfeld, O. J. and Lohan, M. C. and Lu, Y. B. and
29 Masque, P. and McClain, C. R. and Measures, C. and Middag, R. and Moffett, J. and Navidad,
30 A. and Nishioka, J. and Noble, A. and Obata, H. and Ohnemus, D. C. and Owens, S. and
31 Planchon, F. and Pradoux, C. and Puigcorbe, V. and Quay, P. and Radic, A. and Rehkamper,
32 M. and Remenyi, T. and Rijkenberg, M. J. A. and Rintoul, S. and Robinson, L. F. and Roeske,
33 T. and Rosenberg, M. and van der Loeff, M. R. and Ryabenko, E. and Saito, M. A. and
34 Roshan, S. and Salt, L. and Sarthou, G. and Schauer, U. and Scott, P. and Sedwick, P. N. and
35 Sha, L. J. and Shiller, A. M. and Sigman, D. M. and Smethie, W. and Smith, G. J. and Sohrin,
36 Y. and Speich, S. and Stichel, T. and Stutsman, J. and Swift, J. H. and Tagliabue, A. and
37 Thomas, A. and Tsunogai, U. and Twining, B. S. and van Aken, H. M. and van Heuven, S.

1 and van Ooijen, J. and van Weerlee, E. and Venchiarutti, C. and Voelker, A. H. L. and Wake,
2 B. and Warner, M. J. and Woodward, E. M. S. and Wu, J. F. and Wyatt, N. and Yoshikawa, H.
3 and Zheng, X. Y. and Xue, Z. C. and Zieringer, M. and Zimmer, L. A.: The GEOTRACES
4 Intermediate Data Product 2014, Mar Chem, 177, 1-8,
5 <https://doi.org/10.1016/j.marchem.2015.04.005>, 2015.

6 Measures, C. I. and Brown, E. T.: Estimating dust input to the Atlantic Ocean using surface water
7 aluminium concentrations. In: The impact of desert dust across the Mediterranean, Guerzoni,
8 S. and Chester, R. (Eds.), Environmental Science and Technology Library, Springer,
9 Dordrecht, 1996.

10 Measures, C. I. and Vink, S.: On the use of dissolved aluminum in surface waters to estimate dust
11 deposition to the ocean, Global Biogeochem Cy, 14, 317-327,
12 <https://doi.org/10.1029/1999gb001188>, 2000.

13 Menzel Barraqueta, J.-L., Schlosser, C., Planquette, H., Gourain, A., Cheize, M., Boutorh, J., Shelley,
14 R., Pereira, L. C., Gledhill, M., Hopwood, M. J., Lacan, F., Lherminier, P., Sarthou, G., and
15 Achterberg, E. P.: Aluminium in the North Atlantic Ocean and the Labrador Sea
16 (GEOTRACES GA01 section): roles of continental inputs and biogenic particle removal,
17 Biogeosciences, 15, 5271-5286, <https://doi.org/10.5194/bg-15-5271-2018>, 2018.

18 Menzel Barraqueta, J.-L., Klar, J. K., Gledhill, M., Schlosser, C., Shelley, R., Planquette, H. F.,
19 Wenzel, B., Sarthou, G., and Achterberg, E. P.: Atmospheric deposition fluxes over the
20 Atlantic Ocean: a GEOTRACES case study, Biogeosciences, 16, 1525-1542,
21 <https://doi.org/10.5194/bg-16-1525-2019>, 2019.

22 Middag, R., de Baar, H. J. W., Laan, P., and Huhn, O.: The effects of continental margins and water
23 mass circulation on the distribution of dissolved aluminum and manganese in Drake Passage, J
24 Geophys Res-Oceans, 117, C01019, <https://doi.org/10.1029/2011jc007434>, 2012.

25 Milne, A., Schlosser, C., Wake, B. D., Achterberg, E. P., Chance, R., Baker, A. R., Forryan, A., and
26 Lohan, M. C.: Particulate phases are key in controlling dissolved iron concentrations in the
27 (sub)tropical North Atlantic, Geophys Res Lett, 44, 2377-2387,
28 <https://doi.org/10.1002/2016gl072314>, 2017.

29 Mittelstaedt, E.: The upwelling area off Northwest Africa—A description of phenomena related to
30 coastal upwelling, Prog Oceanogr, 12, 307-331, [https://doi.org/10.1016/0079-6611\(83\)90012-](https://doi.org/10.1016/0079-6611(83)90012-5)
31 5, 1983.

32 Mittelstaedt, E.: The ocean boundary along the northwest African coast: Circulation and
33 oceanographic properties at the sea-surface, Prog Oceanogr, 26, 307-355,
34 [https://doi.org/10.1016/0079-6611\(91\)90011-A](https://doi.org/10.1016/0079-6611(91)90011-A), 1991.

35 Moffett, J. W.: The Relationship between cerium and manganese oxidation in the marine environment,
36 Limnol Oceanogr, 39, 1309-1318, <https://doi.org/10.4319/lo.1994.39.6.1309>, 1994.

1 Moffett, J. W. and Ho, J.: Oxidation of cobalt and manganese in seawater via a common microbially
2 catalyzed pathway, *Geochim Cosmochim Ac*, 60, 3415-3424, [https://doi.org/10.1016/0016-](https://doi.org/10.1016/0016-7037(96)00176-7)
3 [7037\(96\)00176-7](https://doi.org/10.1016/0016-7037(96)00176-7), 1996.

4 Moffett, J. W. and Zika, R. G.: Reaction kinetics of hydrogen peroxide with copper and iron in
5 seawater, *Environ Sci Technol*, 21, 804-810, <https://doi.org/10.1021/es00162a012>, 1987.

6 Moffett, J. W., Vedamati, J., Goepfert, T. J., Pratihary, A., Gauns, M., and Naqvi, S. W. A.:
7 Biogeochemistry of iron in the Arabian Sea, *Limnol Oceanogr*, 60, 1671-1688,
8 <https://doi.org/10.1002/lno.10132>, 2015.

9 Moore, C. M., Mills, M. M., Achterberg, E. P., Geider, R. J., LaRoche, J., Lucas, M. I., McDonagh, E.
10 L., Pan, X., Poulton, A. J., Rijkenberg, M. J. A., Suggett, D. J., Ussher, S. J., and Woodward,
11 E. M. S.: Large-scale distribution of Atlantic nitrogen fixation controlled by iron availability,
12 *Nat Geosci*, 2, 867-871, <https://doi.org/10.1038/ngeo667>, 2009.

13 Moore, C. M., Mills, M. M., Arrigo, K. R., Berman-Frank, I., Bopp, L., Boyd, P. W., Galbraith, E. D.,
14 Geider, R. J., Guieu, C., Jaccard, S. L., Jickells, T. D., La Roche, J., Lenton, T. M., Mahowald,
15 N. M., Maranon, E., Marinov, I., Moore, J. K., Nakatsuka, T., Oschlies, A., Saito, M. A.,
16 Thingstad, T. F., Tsuda, A., and Ulloa, O.: Processes and patterns of oceanic nutrient
17 limitation, *Nat Geosci*, 6, 701-710, <https://doi.org/10.1038/Ngeo1765>, 2013.

18 Moore, W. S.: ^{228}Ra in the South-Atlantic Bight, *J Geophys Res-Oceans*, 92, 5177-5190,
19 <https://doi.org/10.1029/JC092iC05p05177>, 1987.

20 Moore, W. S.: Ages of continental shelf waters determined from ^{223}Ra and ^{224}Ra , *J Geophys Res-*
21 *Oceans*, 105, 22117-22122, <https://doi.org/10.1029/1999jc000289>, 2000.

22 Moore, W. S.: Seasonal distribution and flux of radium isotopes on the southeastern U.S. continental
23 shelf, *J Geophys Res*, 112, C10013, <https://doi.org/10.1029/2007JC004199>, 2007.

24 Moore, W. S. and Arnold, R.: Measurement of ^{223}Ra and ^{224}Ra in coastal waters using a delayed
25 coincidence counter, *J Geophys Res*, 101, 1321-1329, <https://doi.org/10.1029/95jc03139>,
26 1996.

27 Moore, W. S. and Cai, P.: Calibration of RaDeCC systems for ^{223}Ra measurements, *Mar Chem*, 156,
28 130-137, <https://doi.org/10.1016/j.marchem.2013.03.002>, 2013.

29 Moran, S. B. and Moore, R. M.: The potential source of dissolved aluminum from resuspended
30 sediments to the North Atlantic Deep Water, *Geochim Cosmochim Ac*, 55, 2745-2751,
31 [https://doi.org/10.1016/0016-7037\(91\)90441-7](https://doi.org/10.1016/0016-7037(91)90441-7), 1991.

32 Morel, F. M. M. and Price, N. M.: The biogeochemical cycles of trace metals in the oceans, *Science*,
33 300, 944-947, <https://doi.org/10.1126/science.1083545>, 2003.

34 Naykki, T., Virtanen, A., Kaukonen, L., Magnusson, B., Vaisanen, T., and Leito, I.: Application of the
35 Nordtest method for "real-time" uncertainty estimation of on-line field measurement, *Environ*
36 *Monit Assess*, 187, 360, <https://doi.org/10.1007/s10661-015-4856-0>, 2015.

1 Ndoye, S., Capet, X., Estrade, P., Sow, B., Dagorne, D., Lazar, A., Gaye, A., and Brehmer, P.: SST
2 patterns and dynamics of the southern Senegal-Gambia upwelling center, *J Geophys Res*
3 *Oceans*, 119, 8315-8335, <https://doi.org/10.1002/2014JC010242>, 2014.

4 Noble, A. E., Lamborg, C. H., Ohnemus, D. C., Lam, P. J., Goepfert, T. J., Measures, C. I., Frame, C.
5 H., Casciotti, K. L., DiTullio, G. R., Jennings, J., and Saito, M. A.: Basin-scale inputs of
6 cobalt, iron, and manganese from the Benguela-Angola front to the South Atlantic Ocean,
7 *Limnol Oceanogr*, 57, 989-1010, <https://doi.org/10.4319/lo.2012.57.4.0989>, 2012.

8 Noble, A. E., Echegoyen-Sanz, Y., Boyle, E. A., Ohnemus, D. C., Lam, P. J., Kayser, R., Reuer, M.,
9 Wu, J. F., and Smethie, W.: Dynamic variability of dissolved Pb and Pb isotope composition
10 from the US North Atlantic GEOTRACES transect, *Deep-Sea Res Pt II*, 116, 208-225,
11 <https://doi.org/10.1016/j.dsr2.2014.11.011>, 2015.

12 Noble, A. E., Ohnemus, D. C., Hawco, N. J., Lam, P. J., and Saito, M. A.: Coastal sources, sinks and
13 strong organic complexation of dissolved cobalt within the US North Atlantic GEOTRACES
14 transect GA03, *Biogeosciences*, 14, 2715-2739, <https://doi.org/10.5194/bg-14-2715-2017>,
15 2017.

16 Noffke, A., Hensen, C., Sommer, S., Scholz, F., Bohlen, L., Mosch, T., Graco, M., and Wallmann, K.:
17 Benthic iron and phosphorus fluxes across the Peruvian oxygen minimum zone, *Limnol*
18 *Oceanogr*, 57, 851-867, <https://doi.org/10.4319/lo.2012.57.3.0851>, 2012.

19 Nriagu, J. O. and Pacyna, J. M.: Quantitative assessment of worldwide contamination of air, water and
20 soils by trace metals, *Nature*, 333, 134-139, <https://doi.org/10.1038/333134a0>, 1988.

21 Nychka, D., Furrer, R., Paige, J., and Sain, S.: fields: Tools for Spatial Data, R package version 8.3-6,
22 <https://CRAN.R-project.org/package=fields>, 2016.

23 Oksanen, J., Blanchet, F. G., Friendly, M., Kindt, R., Legendre, P., McGlenn, D., Minchin, P., B.
24 O'Hara, R., Simpson, G., Solymos, P., Stevens, H., Szöcs, E., and Wagner, H.: vegan:
25 Community Ecology Package. Ordination methods, diversity analysis and other functions for
26 community and vegetation ecologists, version 2.4-4, [https://CRAN.R-](https://CRAN.R-project.org/package=vegan)
27 [project.org/package=vegan](https://CRAN.R-project.org/package=vegan), 2017.

28 Oldham, V. E., Jones, M. R., Tebo, B. M., and Luther, G. W.: Oxidative and reductive processes
29 contributing to manganese cycling at oxic-anoxic interfaces, *Mar Chem*, 195, 122-128,
30 <https://doi.org/10.1016/j.marchem.2017.06.002>, 2017.

31 Orians, K. J. and Bruland, K. W.: Dissolved aluminum in the Central North Pacific, *Nature*, 316, 427-
32 429, <https://doi.org/10.1038/316427a0>, 1985.

33 Orians, K. J. and Bruland, K. W.: The biogeochemistry of aluminum in the Pacific Ocean, *Earth*
34 *Planet Sc Lett*, 78, 397-410, [https://doi.org/10.1016/0012-821x\(86\)90006-3](https://doi.org/10.1016/0012-821x(86)90006-3), 1986.

35 Osborn, T. R.: Estimates of the local rate of vertical diffusion from dissipation measurements, *J Phys*
36 *Oceanogr*, 10, 83-89, [https://doi.org/ 10.1175/1520-0485\(1980\)010<0083:Eotlro>2.0.Co;2](https://doi.org/10.1175/1520-0485(1980)010<0083:Eotlro>2.0.Co;2),
37 1980.

1 Parker, D. L., Morita, T., Mozafarzadeh, M. L., Verity, R., McCarthy, J. K., and Tebo, B. M.: Inter-
2 relationships of MnO₂ precipitation, siderophore-Mn(III) complex formation, siderophore
3 degradation, and iron limitation in Mn(II)-oxidizing bacterial cultures, *Geochim Cosmochim*
4 *Ac*, 71, 5672-5683, <https://doi.org/10.1016/j.gca.2007.03.042>, 2007.

5 Patey, M. D., Achterberg, E. P., Rijkenberg, M. J., and Pearce, R.: Aerosol time-series measurements
6 over the tropical Northeast Atlantic Ocean: Dust sources, elemental composition and
7 mineralogy, *Mar Chem*, 174, 103-119, <https://doi.org/10.1016/j.marchem.2015.06.004>, 2015.

8 Peña-Izquierdo, J., van Sebille, E., Pelegri, J. L., Sprintall, J., Mason, E., Llanillo, P. J., and Machin,
9 F.: Water mass pathways to the North Atlantic oxygen minimum zone, *J Geophys Res-*
10 *Oceans*, 120, 3350-3372, <https://doi.org/10.1002/2014jc010557>, 2015.

11 Rama and Moore, W. S.: Using the radium quartet for evaluating groundwater input and water
12 exchange in salt marshes, *Geochim Cosmochim Ac*, 60, 4645-4652,
13 [https://doi.org/10.1016/S0016-7037\(96\)00289-X](https://doi.org/10.1016/S0016-7037(96)00289-X), 1996.

14 Rapp, I., Schlosser, C., Rusiecka, D., Gledhill, M., and Achterberg, E. P.: Automated preconcentration
15 of Fe, Zn, Cu, Ni, Cd, Pb, Co, and Mn in seawater with analysis using high-resolution sector
16 field inductively-coupled plasma mass spectrometry, *Anal Chim Acta*, 976, 1-13,
17 <https://doi.org/10.1016/j.aca.2017.05.008>, 2017.

18 Rhein, M., Dengler, M., Sültenfuß, J., Hummels, R., Hüttl-Kabus, S., and Bourles, B.: Upwelling and
19 associated heat flux in the equatorial Atlantic inferred from helium isotope disequilibrium, *J*
20 *Geophys Res*, 115, C08021, <https://doi.org/10.1029/2009JC005772>, 2010.

21 Ricciardulli, L. and Wentz, F. J.: Remote Sensing Systems ASCAT C-2015 Daily Ocean Vector
22 Winds on 0.25 deg grid, Version 02.1. Santa Rosa, CA: Remote Sensing Systems. Available at
23 www.remss.com/missions/ascat, 2016.

24 Rijkenberg, M. J. A., Steigenberger, S., Powell, C. F., van Haren, H., Patey, M. D., Baker, A. R., and
25 Achterberg, E. P.: Fluxes and distribution of dissolved iron in the eastern (sub-) tropical North
26 Atlantic Ocean, *Global Biogeochem Cy*, 26, GB3004, <https://doi.org/10.1029/2011gb004264>,
27 2012.

28 Rijkenberg, M. J. A., Middag, R., Laan, P., Gerringa, L. J. A., van Aken, H. M., Schoemann, V., de
29 Jong, J. T. M., and de Baar, H. J. W.: The distribution of dissolved iron in the West Atlantic
30 Ocean, *Plos One*, 9, e101323, <https://doi.org/10.1371/journal.pone.0101323>, 2014.

31 Rudnick, R. L. and Gao, S.: Composition of the continental crust. In: *Treatise on geochemistry*,
32 Holland, H. D. and Turekian, K. K. (Eds.), Pergamon, Oxford, UK, 2006.

33 Rue, E. L., Smith, G. J., Cutter, G. A., and Bruland, K. W.: The response of trace element redox
34 couples to suboxic conditions in the water column, *Deep-Sea Res Pt I*, 44, 113-134,
35 [https://doi.org/10.1016/S0967-0637\(96\)00088-X](https://doi.org/10.1016/S0967-0637(96)00088-X), 1997.

36 Rusiecka, D., Gledhill, M., Milne, A., Achterberg, E. P., Annett, A. L., Atkinson, S., Birchill, A.,
37 Karstensen, J., Lohan, M., Mariez, C., Middag, R., Rolison, J. M., Tanhua, T., Ussher, S., and

1 Connelly, D.: Anthropogenic signatures of lead in the Northeast Atlantic, *Geophys Res Lett*,
2 45, 2734-2743, <https://doi.org/10.1002/2017gl076825>, 2018.

3 Saito, M. A., Goepfert, T. J., and Ritt, J. T.: Some thoughts on the concept of colimitation: Three
4 definitions and the importance of bioavailability, *Limnol Oceanogr*, 53, 276-290,
5 <https://doi.org/10.4319/lo.2008.53.1.0276>, 2008.

6 Saito, M. A., Noble, A. E., Hawco, N., Twining, B. S., Ohnemus, D. C., John, S. G., Lam, P., Conway,
7 T. M., Johnson, R., Moran, D., and McIlvin, M.: The acceleration of dissolved cobalt's
8 ecological stoichiometry due to biological uptake, remineralization, and scavenging in the
9 Atlantic Ocean, *Biogeosciences*, 14, 4637-4662, <https://doi.org/10.5194/bg-14-4637-2017>,
10 2017.

11 Schafstall, J., Dengler, M., Brandt, P., and Bange, H.: Tidal-induced mixing and diapycnal nutrient
12 fluxes in the Mauritanian upwelling region, *J Geophys Res-Oceans*, 115, C10014,
13 <https://doi.org/10.1029/2009jc005940>, 2010.

14 Schlitzer, R. and Anderson, R. F. and Dodas, E. M. and Lohan, M. and Geibert, W. and Tagliabue, A.
15 and Bowie, A. and Jeandel, C. and Maldonado, M. T. and Landing, W. M. and Cockwell, D.
16 and Abadie, C. and Abouchami, W. and Achterberg, E. P. and Agather, A. and Aguliar-Islas,
17 A. and van Aken, H. M. and Andersen, M. and Archer, C. and Auro, M. and de Baar, H. J. and
18 Baars, O. and Baker, A. R. and Bakker, K. and Basak, C. and Baskaran, M. and Bates, N. R.
19 and Bauch, D. and van Beek, P. and Behrens, M. K. and Black, E. and Bluhm, K. and Bopp,
20 L. and Bouman, H. and Bowman, K. and Bown, J. and Boyd, P. and Boye, M. and Boyle, E.
21 A. and Branellec, P. and Bridgestock, L. and Brissebrat, G. and Browning, T. and Bruland, K.
22 W. and Brumsack, H.-J. and Brzezinski, M. and Buck, C. S. and Buck, K. N. and Buesseler,
23 K. and Bull, A. and Butler, E. and Cai, P. and Mor, P. C. and Cardinal, D. and Carlson, C. and
24 Carrasco, G. and Casacuberta, N. and Casciotti, K. L. and Castrillejo, M. and Chamizo, E. and
25 Chance, R. and Charette, M. A. and Chaves, J. E. and Cheng, H. and Chever, F. and Christl,
26 M. and Church, T. M. and Closset, I. and Colman, A. and Conway, T. M. and Cossa, D. and
27 Croot, P. and Cullen, J. T. and Cutter, G. A. and Daniels, C. and Dehairs, F. and Deng, F. and
28 Dieu, H. T. and Duggan, B. and Dulaquais, G. and Dumousseaud, C. and Echevoyen-Sanz, Y.
29 and Edwards, R. L. and Ellwood, M. and Fahrback, E. and Fitzsimmons, J. N. and Russell
30 Flegel, A. and Fleisher, M. Q. and van de Flierdt, T. and Frank, M. and Friedrich, J. and
31 Fripiat, F. and Fröllje, H. and Galer, S. J. G. and Gamo, T. and Ganeshram, R. S. and Garcia-
32 Orellana, J. and Garcia-Solsona, E. and Gault-Ringold, M. and George, E. and Gerringa, L. J.
33 A. and Gilbert, M. and Godoy, J. M. and Goldstein, S. L. and Gonzalez, S. R. and Grissom, K.
34 and Hammerschmidt, C. and Hartman, A. and Hassler, C. S. and Hathorne, E. C. and Hatta,
35 M. and Hawco, N. and Hayes, C. T. and Heimbürger, L.-E. and Helgoe, J. and Heller, M. and
36 Henderson, G. M. and Henderson, P. B. and van Heuven, S. and Ho, P. and Horner, T. J. and
37 Hsieh, Y.-T. and Huang, K.-F. and Humphreys, M. P. and Isshiki, K. and Jacquot, J. E. and

1 Janssen, D. J. and Jenkins, W. J. and John, S. and Jones, E. M. and Jones, J. L. and Kadko, D.
2 C. and Kayser, R. and Kenna, T. C. and Khondoker, R. and Kim, T. and Kipp, L. and Klar, J.
3 K. and Klunder, M. and Kretschmer, S. and Kumamoto, Y. and Laan, P. and Labatut, M. and
4 Lacan, F. and Lam, P. J. and Lambelet, M. and Lamborg, C. H. and Le Moigne, F. A. C. and
5 Le Roy, E. and Lechtenfeld, O. J. and Lee, J.-M. and Lherminier, P. and Little, S. and López-
6 Lora, M. and Lu, Y. and Masque, P. and Mawji, E. and McClain, C. R. and Measures, C. and
7 Mehic, S. and Barraqueta, J.-L. M. and van der Merwe, P. and Middag, R. and Mieruch, S.
8 and Milne, A. and Minami, T. and Moffett, J. W. and Moncoiffe, G. and Moore, W. S. and
9 Morris, P. J. and Morton, P. L. and Nakaguchi, Y. and Nakayama, N. and Niedermiller, J. and
10 Nishioka, J. and Nishiuchi, A. and Noble, A. and Obata, H. and Ober, S. and Ohnemus, D. C.
11 and van Ooijen, J. and O'Sullivan, J. and Owens, S. and Pahnke, K. and Paul, M. and Pavia, F.
12 and Pena, L. D. and Peters, B. and Planchon, F. and Planquette, H. and Pradoux, C. and
13 Puigcorb , V. and Quay, P. and Queroue, F. and Radic, A. and Rauschenberg, S. and
14 Rehk mper, M. and Rember, R. and Remenyi, T. and Resing, J. A. and Rickli, J. and Rigaud,
15 S. and Rijkenberg, M. J. A. and Rintoul, S. and Robinson, L. F. and Roca-Mart , M. and
16 Rodellas, V. and Roeske, T. and Rolison, J. M. and Rosenberg, M. and Roshan, S. and Rutgers
17 van der Loeff, M. M. and Ryabenko, E. and Saito, M. A. and Salt, L. A. and Sanial, V. and
18 Sarthou, G. and Schallenberg, C. and Schauer, U. and Scher, H. and Schlosser, C. and
19 Schnetger, B. and Scott, P. and Sedwick, P. N. and Semiletov, I. and Shelley, R. and Sherrell,
20 R. M. and Shiller, A. M. and Sigman, D. M. and Singh, S. K. and Slagter, H. A. and Slater, E.
21 and Smethie, W. M. and Snaith, H. and Sohrin, Y. and Sohst, B. and Sonke, J. E. and Speich,
22 S. and Steinfeldt, R. and Stewart, G. and Stichel, T. and Stirling, C. H. and Stutsman, J. and
23 Swarr, G. J. and Swift, J. H. and Thomas, A. and Thorne, K. and Till, C. P. and Till, R. and
24 Townsend, A. T. and Townsend, E. and Tuerena, R. and Twining, B. S. and Vance, D. and
25 Velazquez, S. and Venchiarutti, C. and Villa-Alfageme, M. and Vivancos, S. M. and Voelker,
26 A. H. L. and Wake, B. and Warner, M. J. and Watson, R. and van Weerlee, E. and Alexandra
27 Weigand, M. and Weinstein, Y. and Weiss, D. and Wisotzki, A. and Woodward, E. M. S. and
28 Wu, J. and Wu, Y. and Wuttig, K. and Wyatt, N. and Xiang, Y. and Xie, R. C. and Xue, Z. and
29 Yoshikawa, H. and Zhang, J. and Zhang, P. and Zhao, Y. and Zheng, L. and Zheng, X.-Y. and
30 Zieringer, M. and Zimmer, L. A. and Ziveri, P. and Zunino, P. and Zurbrick, C.: The
31 GEOTRACES Intermediate Data Product 2017, *Chem Geol*, 493, 210-223,
32 <https://doi.org/10.1016/j.chemgeo.2018.05.040>, 2018.

33 Schlosser, C., Streu, P., Frank, M., Lavik, G., Croot, P. L., Dengler, M., and Achterberg, E. P.: H₂S
34 events in the Peruvian oxygen minimum zone facilitate enhanced dissolved Fe concentrations,
35 *Sci Rep*, 8, <https://doi.org/10.1038/s41598-018-30580-w>, 2018.

36 Schmidtko, S., Stramma, L., and Visbeck, M.: Decline in global oceanic oxygen content during the
37 past five decades, *Nature*, 542, 335-339, <https://doi.org/10.1038/nature21399>, 2017.

1 Scholten, J. C., Pham, M. K., Blinova, O., Charette, M. A., Dulaiova, H., and Eriksson, M.:
2 Preparation of Mn-fiber standards for the efficiency calibration of the delayed coincidence
3 counting system (RaDeCC), *Mar Chem*, 121, 206-214,
4 <https://doi.org/10.1016/j.marchem.2010.04.009>, 2010.

5 Scholz, F., Loscher, C. R., Fiskal, A., Sommer, S., Hensen, C., Lomnitz, U., Wuttig, K., Gottlicher, J.,
6 Kossel, E., Steininger, R., and Canfield, D. E.: Nitrate-dependent iron oxidation limits iron
7 transport in anoxic ocean regions, *Earth Planet Sc Lett*, 454, 272-281,
8 <https://doi.org/10.1016/j.epsl.2016.09.025>, 2016.

9 Schroller-Lomnitz, U., Hensen, C., Dale, A. W., Scholz, F., Clemens, D., Sommer, S., Noffke, A., and
10 Wallmann, K.: Dissolved benthic phosphate, iron and carbon fluxes in the Mauritanian
11 upwelling system and implications for ongoing deoxygenation, *Deep-Sea Res Pt I*, 143, 70-84,
12 <https://doi.org/10.1016/j.dsr.2018.11.008>, 2019.

13 Severmann, S., McManus, J., Berelson, W. M., and Hammond, D. E.: The continental shelf benthic
14 iron flux and its isotope composition, *Geochim Cosmochim Ac*, 74, 3984-4004,
15 <https://doi.org/10.1016/j.gca.2010.04.022>, 2010.

16 Shelley, R. U., Morton, P. L., and Landing, W. M.: Elemental ratios and enrichment factors in aerosols
17 from the US-GEOTRACES North Atlantic transects, *Deep-Sea Res Pt II*, 116, 262-272,
18 <https://doi.org/10.1016/j.dsr2.2014.12.005>, 2015.

19 Shelley, R. U., Landing, W. M., Ussher, S. J., Planquette, H., and Sarthou, G.: Regional trends in the
20 fractional solubility of Fe and other metals from North Atlantic aerosols (GEOTRACES
21 cruises GA01 and GA03) following a two-stage leach, *Biogeosciences*, 15, 2271-2288,
22 <https://doi.org/10.5194/bg-15-2271-2018>, 2018.

23 Sherrell, R. M. and Boyle, E. A.: The trace metal composition of suspended particles in the oceanic
24 water column near Bermuda, *Earth Planet Sc Lett*, 111, 155-174, [https://doi.org/10.1016/0012-821x\(92\)90176-V](https://doi.org/10.1016/0012-821x(92)90176-V), 1992.

26 Soataert, K., Petzoldt, T., and Meysman, F.: marelac: Tools for Aquatic Sciences, Version 2.1.6,
27 <https://CRAN.R-project.org/package=marelac>, 2016.

28 Sommer, S., Dengler, M., and Treude, T.: Benthic element cycling, fluxes and transport of solutes
29 across the benthic boundary layer in the Mauritanian oxygen minimum zone, (SFB754) –
30 Cruise No. M107 – May 30 – July 03, 2014 – Fortaleza (Brazil) – Las Palmas (Spain),
31 METEOR-Berichte, M107, DFG-Senatskommission für Ozeanographie,
32 https://doi.org/10.2312/cr_m107, 2015.

33 Steinfeldt, R., Sultenfuss, J., Dengler, M., Fischer, T., and Rhein, M.: Coastal upwelling off Peru and
34 Mauritania inferred from helium isotope disequilibrium, *Biogeosciences*, 12, 7519-7533,
35 <https://doi.org/10.5194/bg-12-7519-2015>, 2015.

1 Stramma, L., Brandt, P., Schafstall, J., Schott, F., Fischer, J., and Kortzinger, A.: Oxygen minimum
2 zone in the North Atlantic south and east of the Cape Verde Islands, *J Geophys Res-Oceans*,
3 113, C04014, <https://doi.org/10.1029/2007jc004369>, 2008a.

4 Stramma, L., Johnson, G. C., Sprintall, J., and Mohrholz, V.: Expanding oxygen-minimum zones in
5 the tropical oceans, *Science*, 320, 655-658, <https://doi.org/10.1126/science.1153847>, 2008b.

6 Stumm, W. and Morgan, J. J.: *Aquatic Chemistry: Chemical Equilibria and Rates in Natural Waters*,
7 John Wiley & Sons, New York, 1995.

8 Sunda, W. G. and Huntsman, S. A.: Effect of sunlight on redox cycles of manganese in the
9 Southwestern Sargasso Sea, *Deep-Sea Res*, 35, 1297-1317, [https://doi.org/10.1016/0198-](https://doi.org/10.1016/0198-0149(88)90084-2)
10 [0149\(88\)90084-2](https://doi.org/10.1016/0198-0149(88)90084-2), 1988.

11 Sunda, W. G. and Huntsman, S. A.: Photoreduction of manganese oxides in seawater, *Mar Chem*, 46,
12 133-152, [https://doi.org/10.1016/0304-4203\(94\)90051-5](https://doi.org/10.1016/0304-4203(94)90051-5), 1994.

13 Tanhua, T., and Liu, M.: Upwelling velocity and ventilation in the Mauritanian upwelling system
14 estimated by CFC-12 and SF₆ observations, *J Mar Sys*, 151, 57-70,
15 <https://doi.org/10.1016/j.jmarsys.2015.07.002>, 2015.

16 Tebo, B. M. and Emerson, S.: Microbial manganese(II) oxidation in the marine environment: a
17 quantitative study, *Biogeochemistry*, 2, 149-161, <https://doi.org/10.1007/Bf02180192>, 1986.

18 Tebo, B. M., Bargar, J. R., Clement, B. G., Dick, G. J., Murray, K. J., Parker, D., Verity, R., and
19 Webb, S. M.: Biogenic manganese oxides: Properties and mechanisms of formation, *Annu*
20 *Rev Earth Pl Sc*, 32, 287-328, <https://doi.org/10.1146/annurev.earth.32.101802.120213>, 2004.

21 Thomsen, S., Karstensen, J., Kiko, R., Krahnemann, G., Dengler, M., and Engel, A.: Remote and local
22 drivers of oxygen and nitrate variability in the shallow oxygen minimum zone off Mauritania
23 in June 2014, *Biogeosciences*, 16, 979-998, <https://doi.org/10.5194/bg-16-979-2019>, 2019.

24 Tomczak, M.: An analysis of mixing in the frontal zone of South and North Atlantic Central Water off
25 North-West Africa, *Prog Oceanogr*, 10, 173-192, [https://doi.org/10.1016/0079-](https://doi.org/10.1016/0079-6611(81)90011-2)
26 [6611\(81\)90011-2](https://doi.org/10.1016/0079-6611(81)90011-2), 1981.

27 Tweddle, J. F., Sharples, J., Palmer, M. R., Davidson K., and McNeill, S.: Enhanced nutrient fluxes at
28 the shelf sea seasonal thermocline caused by stratified flow over a bank, *Prog Oceanogr*, 117,
29 37-47, <https://doi.org/10.1016/j.pocean.2013.06.018>, 2013.

30 Twining, B. S., Rauschenberg, S., Morton, P. L., and Vogt, S.: Metal contents of phytoplankton and
31 labile particulate material in the North Atlantic Ocean, *Prog Oceanogr*, 137, 261-283,
32 <https://doi.org/10.1016/j.pocean.2015.07.001>, 2015.

33 Ussher, S. J., Achterberg, E. P., Powell, C., Baker, A. R., Jickells, T. D., Torres, R., and Worsfold, P.
34 J.: Impact of atmospheric deposition on the contrasting iron biogeochemistry of the North and
35 South Atlantic Ocean, *Global Biogeochem Cy*, 27, 1096-1107,
36 <https://doi.org/10.1002/gbc.20056>, 2013.

- 1 Verhoef, A., Portabella, M., and Stoffelen, A.: High resolution ASCAT scatterometer winds near the
2 coast, *IEEE, Trans Geosci Remote Sens*, 50, 2481-248,
3 <https://doi.org/10.1109/TGRS.2011.2175001>, 2012.
- 4 Véron, A., Patterson, C., and Flegal, A.: Use of stable lead isotopes to characterize the sources of
5 anthropogenic lead in North Atlantic surface waters, *Geochim Cosmochim Ac*, 58, 3199-3206,
6 [https://doi.org/10.1016/0016-7037\(94\)90047-7](https://doi.org/10.1016/0016-7037(94)90047-7), 1994.
- 7 von Langen, P. J., Johnson, K. S., Coale, K. H., and Elrod, V. A.: Oxidation kinetics of manganese(II)
8 in seawater at nanomolar concentrations, *Geochim Cosmochim Ac*, 61, 4945-4954,
9 [https://doi.org/10.1016/S0016-7037\(97\)00355-4](https://doi.org/10.1016/S0016-7037(97)00355-4), 1997.
- 10 Weiss, R. F.: The solubility of nitrogen, oxygen and argon in water and seawater, *Deep Sea Res and*
11 *Oceanographic Abstracts*, 17, 721-735, [https://doi.org/10.1016/0011-7471\(70\)90037-9](https://doi.org/10.1016/0011-7471(70)90037-9), 1970.
- 12 Winkler, L. W.: Bestimmung des im Wasser gelösten Sauerstoffs, *Ber Dtsch Chem Ges*, 21, 2843-
13 2855, <https://doi.org/10.1002/cber.188802102122>, 1888.
- 14 Wu, J. F. and Luther, G. W.: Size-fractionated iron concentrations in the water column of the western
15 North Atlantic Ocean, *Limnol Oceanogr*, 39, 1119-1129,
16 <https://doi.org/10.4319/lo.1994.39.5.1119>, 1994.
- 17 Wuttig, K., Heller, M. I., and Croot, P. L.: Pathways of Superoxide (O_2^-) Decay in the Eastern Tropical
18 North Atlantic, *Environ Sci Technol*, 47(18), 10249-10256, <https://doi.org/10.1021/es401658t>,
19 2013.
- 20 Wyrтки, K.: The oxygen minima in relation to ocean circulation, *Deep-Sea Res*, 9, 11-23,
21 [https://doi.org/10.1016/0011-7471\(62\)90243-7](https://doi.org/10.1016/0011-7471(62)90243-7), 1962.
- 22 Yücel, M., Beaton, A. D., Dengler, M., Mowlem, M. C., Sohl, F., and Sommer, S.: Nitrate and Nitrite
23 Variability at the Seafloor of an Oxygen Minimum Zone Revealed by a Novel Microfluidic In-
24 Situ Chemical Sensor, *PLoS ONE* 10(7), e0132785,
25 <https://doi.org/10.1371/journal.pone.0132785>, 2015.
- 26 Zenk, W., Klein, B., and Schroder, M.: Cape-Verde Frontal Zone, *Deep-Sea Res*, 38, S505-S530,
27 [https://doi.org/10.1016/S0198-0149\(12\)80022-7](https://doi.org/10.1016/S0198-0149(12)80022-7), 1991.

28

1 **Table 1.** Analyzed reference seawater, procedural blanks and detection limits (three times the standard
 2 deviation of the blank). Mean values and standard deviation for Cd, Pb, Fe, Ni, Cu, Mn and Co and
 3 available consensus values (± 1 standard deviation), n = number of measurements.

	SAFe S (nmol L ⁻¹) n=11	SAFe S consensus value (nmol L ⁻¹)	SAFe D2 (nmol L ⁻¹) n=7	SAFe D2 consensus value (nmol L ⁻¹)	Blank (pmol L ⁻¹)	Detection limit (pmol L ⁻¹)
Cd	0.003 \pm 0.002	0.001	1.089 \pm 0.043	1.011 \pm 0.024	2.2 \pm 0.3	0.8
Pb	0.050 \pm 0.003	0.049 \pm 0.002	0.028 \pm 0.001	0.029 \pm 0.002	0.4 \pm 0.2	0.6
Fe	0.091 \pm 0.009	0.095 \pm 0.008	1.029 \pm 0.038	0.956 \pm 0.024	68 \pm 10	29
Ni	2.415 \pm 0.086	2.34 \pm 0.09	9.625 \pm 0.175	8.85 \pm 0.26	112 \pm 20	59
Cu	0.514 \pm 0.037	0.53 \pm 0.05	2.176 \pm 0.152	2.34 \pm 0.15	14 \pm 3	9.3
Co	0.005 \pm 0.001	0.005 \pm 0.001	0.048 \pm 0.003	0.047 \pm 0.003	2.7 \pm 0.8	2.5
Mn	0.814 \pm 0.033	0.810 \pm 0.062	0.437 \pm 0.029	0.36 \pm 0.05	14 \pm 6	17

4

5

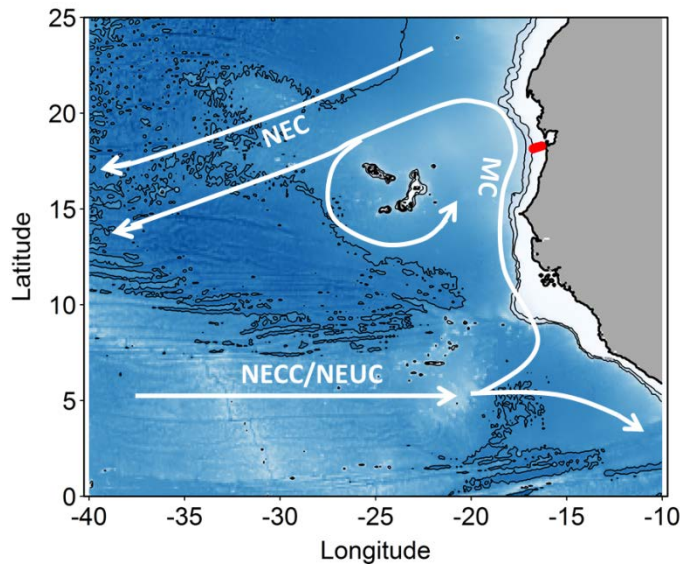
6

7 **Table 1.** TM/Al ratios of different fractions for
 8 the repeated deployments at station 3 within the
 9 OMZ below 50 m water depth.

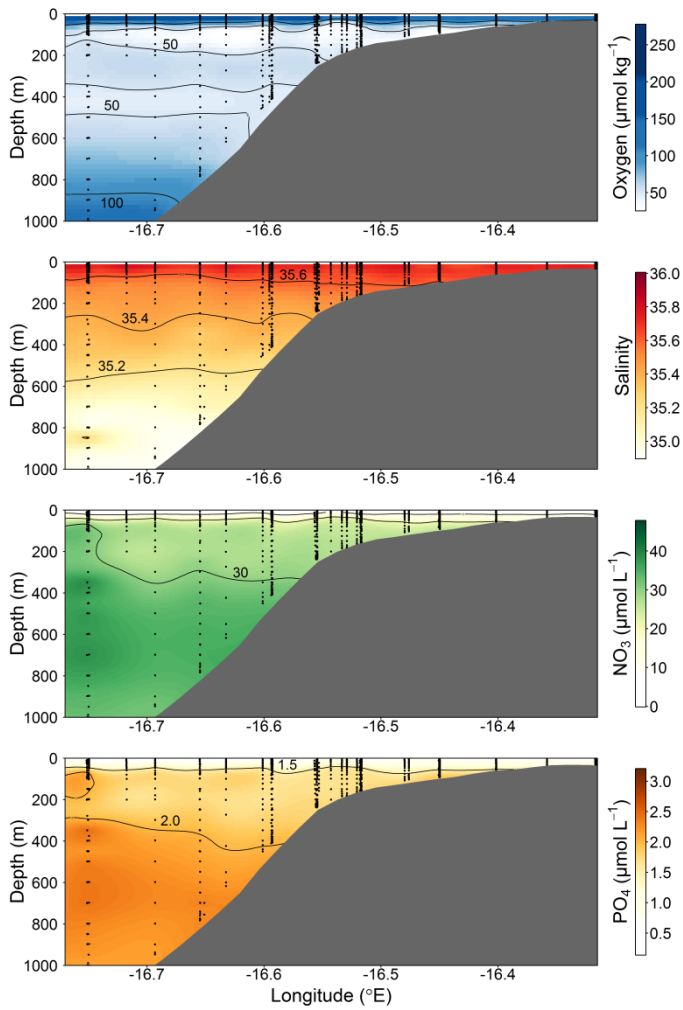
Parameter	Stn 3A	Stn 3B
dFe/dAl	0.38–0.79	0.35–0.37
TDFe/TDAI	4.00–13.42	1.83–2.81
LpFe/LpAl	10.00–29.50	3.64–8.59
dCo/dAl	0.009–0.011	0.009–0.011
TDCo/TDAI	0.009–0.010	0.006–0.008
LpCo/LpAl	0.007–0.011	0.001–0.005
dMn/dAl	0.26–0.45	0.19–0.21
TDMn/TDAI	0.26–0.32	0.12–0.17
LpMn/LpAl	0.14–0.28	0.02–0.09

10

11

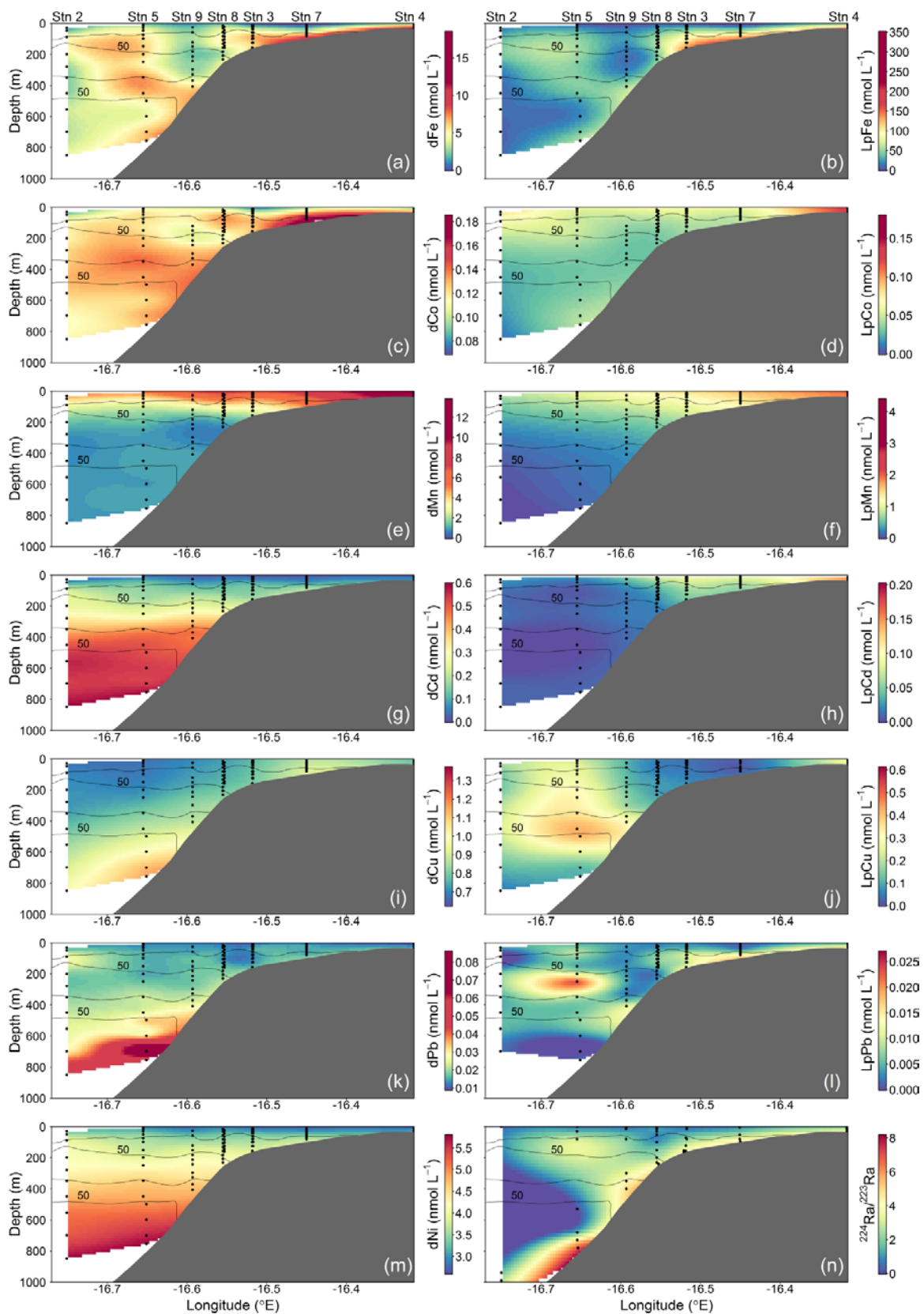


1
2 **Figure 1.** Map of the study area. Stations along the transect during M107 (June 2014) are displayed in
3 red circles and major currents in white lines (adapted from Brandt et al. 2015). MC = Mauritania
4 Current; NEC = North Equatorial Current; NECC = North Equatorial Countercurrent; NEUC = North
5 Equatorial Undercurrent.
6

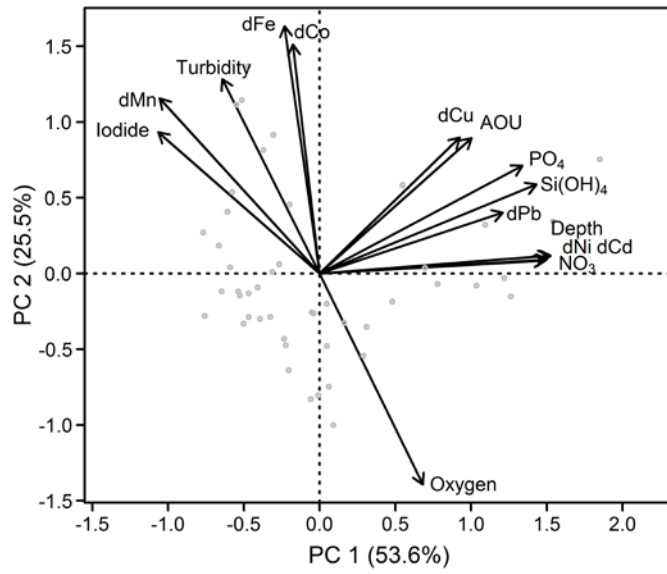


1
 2 **Figure 2.** Section plots of oxygen ($\mu\text{mol kg}^{-1}$), salinity (PSU), NO_3 ($\mu\text{mol L}^{-1}$) and PO_4 ($\mu\text{mol L}^{-1}$)
 3 along the transect off the Mauritanian coast in June 2014.

4

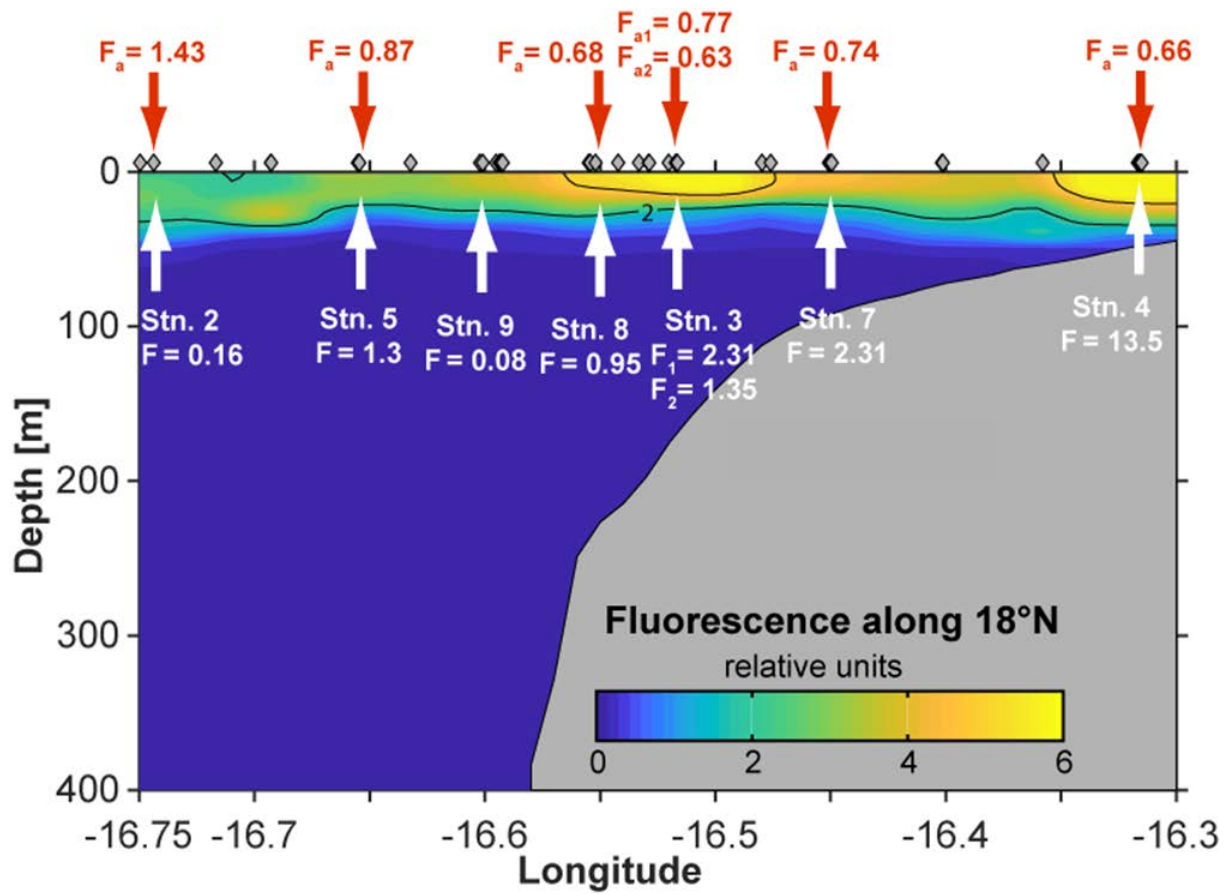


1
 2 **Figure 3.** Spatial distributions of dissolved (d) and leachable particulate (Lp) trace metals and
 3 $^{224}\text{Ra}/^{223}\text{Ra}$ across the Mauritanian shelf at $18^{\circ}20'N$ in June 2014. Each sample location is indicated as
 4 black dot and oxygen contours at $50 \mu\text{mol kg}^{-1}$ enclosing the upper and lower OMZ are displayed as
 5 black contour lines.

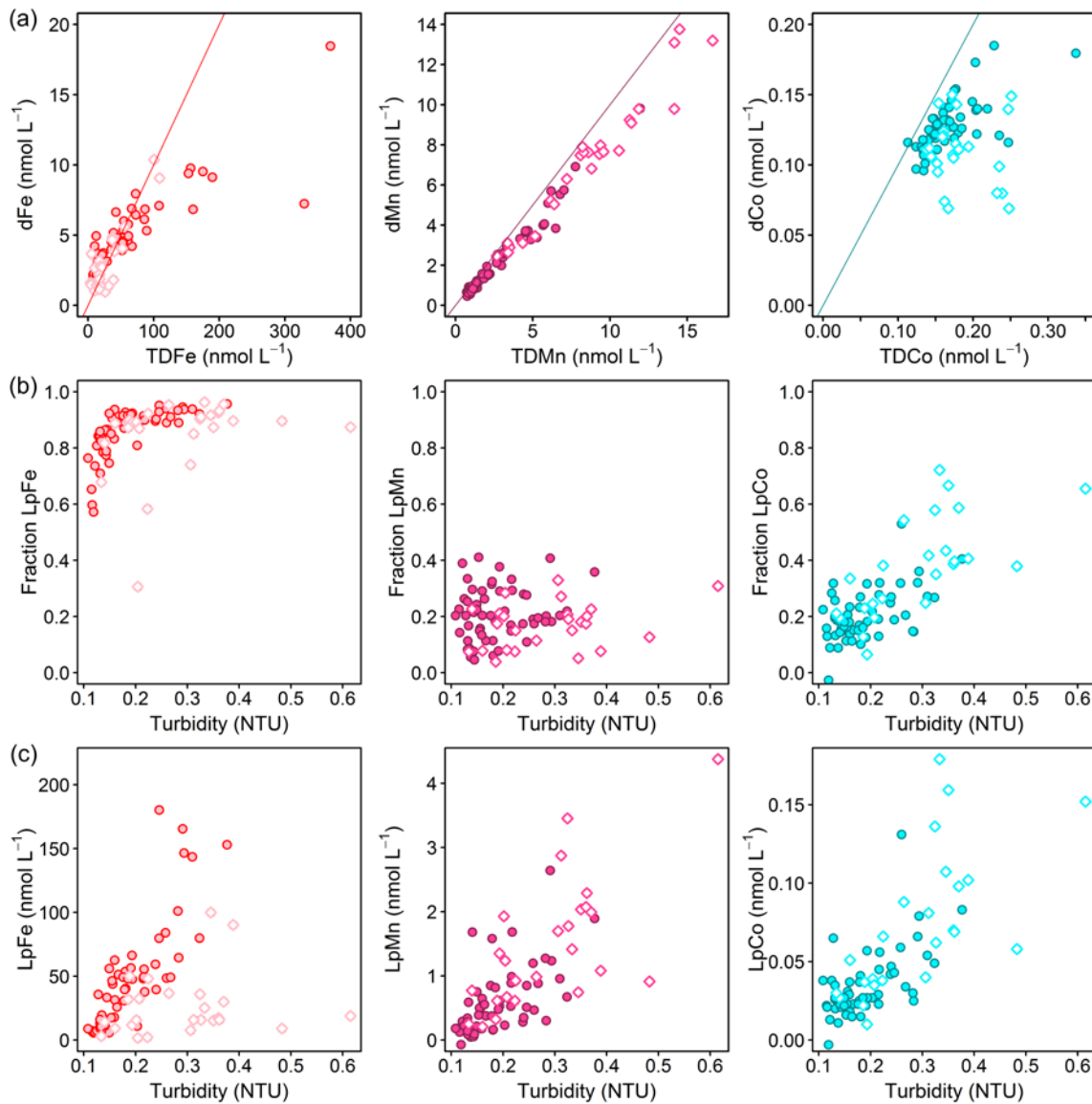


1
 2 **Figure 4.** Principal component analysis of the Mauritanian shelf data set. Principal component
 3 loadings for each variable are indicated by black vectors. Component scores of each sample are
 4 indicated as grey circles. Loadings/scores have been scaled symmetrically by square root of the
 5 eigenvalue.

6

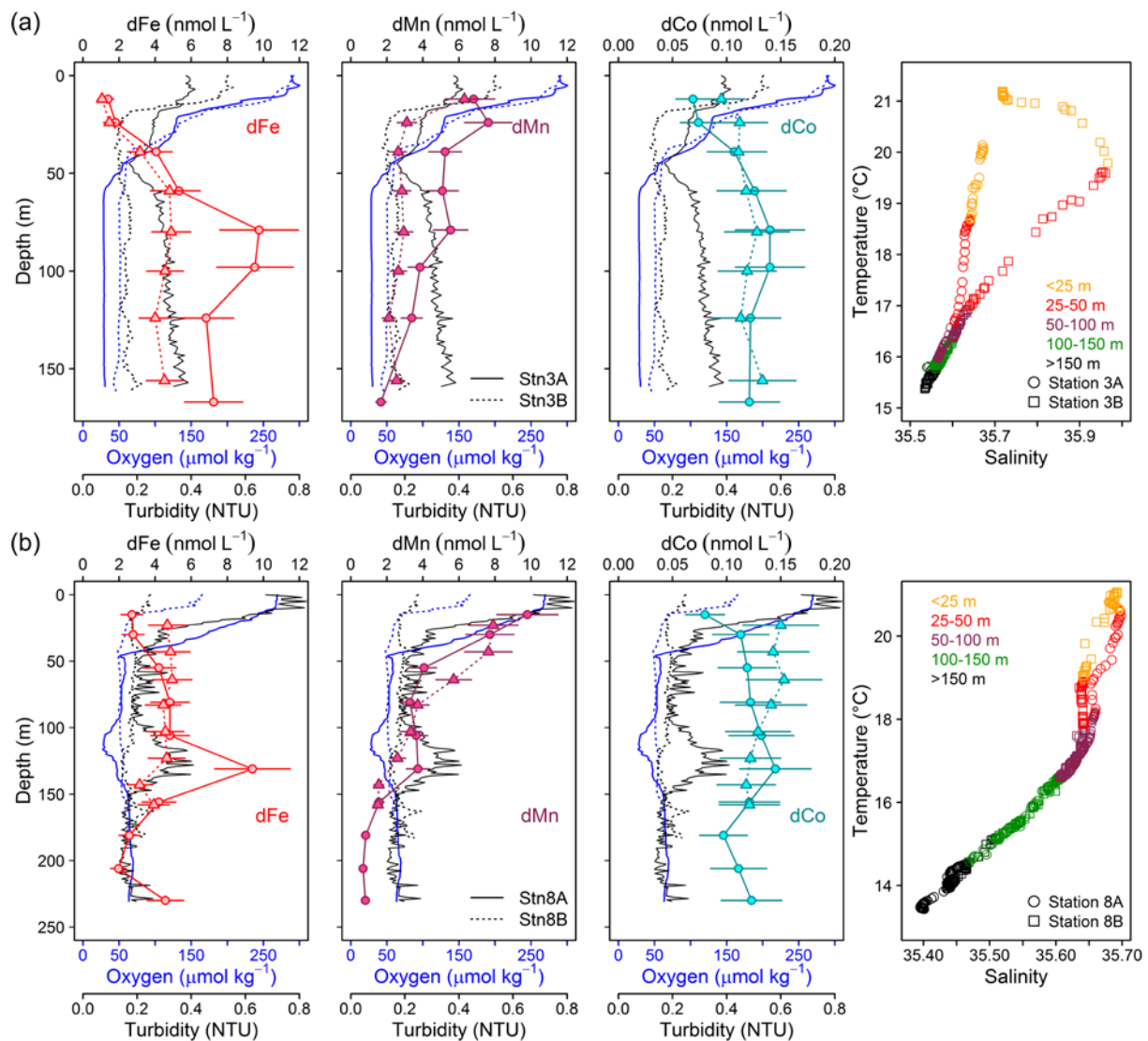


1
 2 **Figure 5.** Atmospheric dFe fluxes (F_a ; red) and vertical dFe fluxes (F ; white) in $\mu\text{mol m}^{-2} \text{d}^{-1}$ along the
 3 transect at 18°20'N in June 2014.
 4



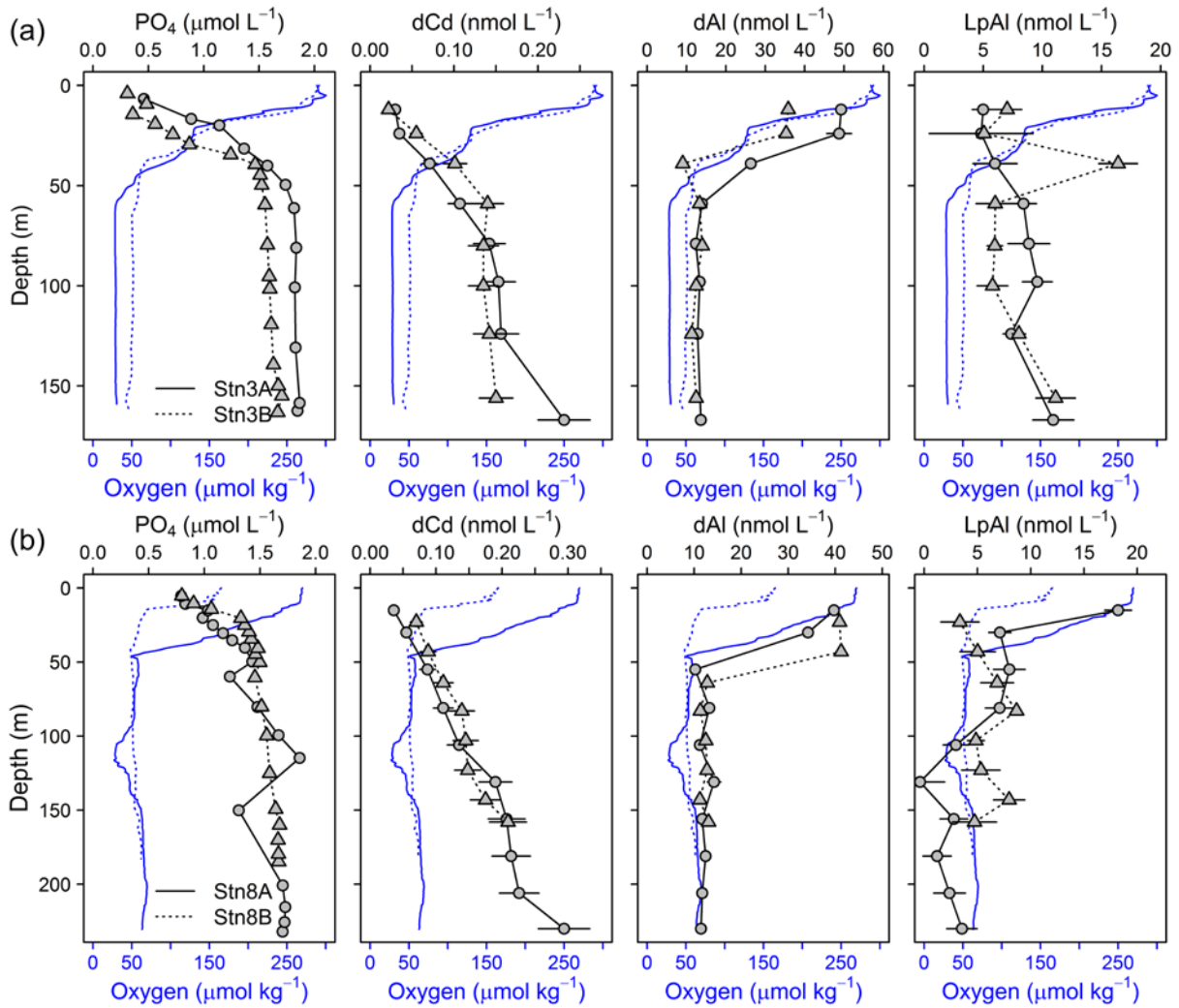
1
 2 **Figure 6.** (a) Dissolved against total dissolvable trace metal concentrations for Fe (left; red line: TDFe
 3 = 10*dFe), Mn (middle; purple line: TDMn = dMn) and Co (right; turquoise line: TDCo = dCo). (b)
 4 Fraction of leachable particulate trace metals (Lp/TD) against turbidity and (c) Leachable particulate
 5 concentrations against turbidity for Fe (left), Mn (middle) and Co (right). Filled circles display all data
 6 points below 50 m depth, open diamonds at depths shallower than 50 m.

7



1
 2 **Figure 7.** Repeat stations: oxygen concentration, turbidity and dissolved trace metals (Fe, Mn and Co)
 3 and temperature vs salinity plots. First deployment displayed as solid line and circles and second
 4 deployment displayed as dashed line and triangles. (a) Station 3 (18.23°N, 16.52°W, 170 m water
 5 depth, 9 days between deployments). (b) Station 8 (18.22°N, 16.55°N, 189–238 m water depth, 2 days
 6 between deployments).

7



1
2 **Figure 8.** Depth profiles of dCd, PO₄, dAl and LpAl of repeat stations. First deployment displayed as
3 solid black line and circles and second deployment displayed as dashed black line and triangles.
4 Oxygen concentrations are indicated as blue solid line for the first deployment and dashed blue line for
5 the second deployment. (a) Station 3 (18.23°N, 16.52°W, 170 m water depth, 9 days between
6 deployments and (b) Station 8 (18.22°N, 16.55°W, 189–238 m water depth, 2 days between
7 deployments).

8